STREAM AQUIFER INTERACTIONS: ANALYTICAL SOLUTION TO ESTIMATE STREAM DEPLETIONS CAUSED BY STREAM STAGE FLUCTUATIONS AND PUMPING WELLS NEAR STREAMS

A Dissertation

by

TRIN INTARAPRASONG

Submitted to the Office of Graduate Studies of
Texas A&M University
in partial fulfillment of the requirements for the degree of

DOCTOR OF PHILOSOPHY

December 2007

Major Subject: Geology

STREAM AQUIFER INTERACTIONS: ANALYTICAL SOLUTION TO ESTIMATE STREAM DEPLETIONS CAUSED BY STREAM STAGE FLUCTUATIONS AND PUMPING WELLS NEAR STREAMS

A Dissertation

by

TRIN INTARAPRASONG

Submitted to the Office of Graduate Studies of
Texas A&M University
in partial fulfillment of the requirements for the degree of

DOCTOR OF PHILOSOPHY

Approved by:

Chair of Committee,	Hongbin Zhan
Committee Members,	Chris Mathewson
	David Sparks
	Jennifer McGuire
	Yalchin Efendiev
Head of Department,	Andreas Kronenberg

December 2007

Major Subject: Geology

ABSTRACT

Stream Aquifer Interactions: Analytical Solution to Estimate Stream Depletions Caused by Stream Stage Fluctuations and Pumping Wells near Streams. (December 2007)

Trin Intaraprasong, B.S., University of California, Santa Cruz

Chair of Advisory Committee: Dr. Hongbin Zhan

This dissertation is composed of three parts of contributions. Systems of a fully penetrating pumping well in a confined aquifer near a fully penetrating stream with and without streambeds are discussed in Chapter II. In Chapter III, stream-aquifer systems with a fully penetrating pumping well in a confined aquifer between two parallel fully penetrating streams with and without streambeds are discussed. Stream depletion rates in Chapter II are solved using Laplace and Fourier transform methods, and stream depletion rates in Chapter III are solved using the potential method.

Chapter II presents analytical solutions in the Laplace domain for general stream depletion rates caused by a pumping well and caused by stream stage fluctuations. For seasonal case, the stream stage is a function of time. For an individual flood wave, the stream stage is a function of time and distance along the stream. Semi-analytical solutions of seasonal stream depletion rates in time domain, using a cosine function to simulate stream stage fluctuations, are presented. The stream depletion rate caused by pumping is solved analytically, while the stream depletion rate caused by stream stage fluctuations is solved numerically. Various parameters affecting stream depletion rates,

such as flood period and streambed, are analyzed. For a short-term case, the pumping rate is assumed to be constant, and a Gaussian function is used as an example of floodwaves. This part is solved using the same method as used in the seasonal case. Early time and late time approximations of the stream depletion rates are also presented. This approximation leads to an interesting finding that the stream depletion rate caused by seasonal stream stage fluctuations can be neglected if the stream aquifer system has a long time to equilibrate. In Chapter III, analytical stream depletion rates caused by a pumping well between two parallel streams with and without streambeds are presented. In this chapter, stream stage is assumed to be constant. Capture zone delineations were analyzed in the case without streambed. For the case with streambed, streambed conductance, which is an important factor controlling stream depletion, is analyzed.

All solutions discussed in this dissertation can be used to predict stream depletion rates and to estimate parameters controlling stream depletion rates, which is crucial for water management. In addition to the stream depletion, the derived semi-analytical solutions in the Laplace-Fourier domain can also be used to predict drawdown in the aquifer near the stream. The derived solutions may also be used inversely to find the streambed and aquifer parameters if the stream stage fluctuation can be well described.

DEDICATION

To my parents

ACKNOWLEDGEMENTS

I am grateful for the help and support of my committee members. I cannot express my gratitude in words to Dr. Hongbin Zhan, my graduate advisor, for everything he did for me. I express gratitude to Dr. McGuire, Dr. Mathewson, and Dr. Sparks for their valuable time and comments. I express thanks to Dr. Efendiev and Dr. Cunningham for helping me with math and programming problems. I would like to thank many former teachers who taught me many valuable lessons.

I appreciate my family for their support. I thank my father for teaching me the value of honesty. I thank my mother for teaching me persistence and hard work. I thank my brother for being a good role model for me when I was young. I thank my relatives and my mom's friends for their help and support.

I express my gratitude toward my friends and colleagues, Yuttapong Jiraraksopokun, for help with matlab codes and, Dr. Dongmin Sun, for all her help.

NOMENCLATURE

m	meter
d	day
hr	hour

List of symbols used in Chapter II.

A	amplitude of the flood wave [m]
A_0	a factor related to amplitude of the flood wave [m^2]
B	aquifer thickness [m]
B'	streambed thickness [m]
D	a factor related to width of the floodwave [m^2/d],
f_y	frequency function [-]
h	hydraulic head in the aquifer [m]
h_o	initial hydraulic head in the aquifer [m]
h_s	hydraulic head in the stream [m]
H_s	drawdown in the stream [m]
J_o	Bessel function of the first kind [-]
k	hydraulic conductivity of streambed [m/d]
K	hydraulic conductivity of aquifer [m/d]
p	Laplace transform parameter [-]
q	stream depletion per unit river width [m^2/d]

q_1	stream depletion per unit river width caused by stream stage fluctuation [m^2/d]
q_2	stream depletion per unit river width caused by pumping [m^2/d]
Q_W	pumping rate as a function of time[m^3/d].
Q_o	constant pumping rate [m^3/d].
Q_T	total stream depletion [m^3/d]
Q_1	stream depletion caused by stream stage fluctuations [m^3/d]
Q_2	stream depletion caused by pumping [m^3/d]
s	drawdown in the aquifer [m]
s_1	drawdown in the aquifer caused by stream stage fluctuations [m]
s_2	drawdown in the aquifer caused by pumping [m]
S_s'	specific storage of streambed [m^{-1}]
S_s	specific storage of aquifer [m^{-1}]
t	time [d].
t_0	time which a pumping well starts [d]
t_s	time which a pumping well stop [d]
v	factor relate to velocity of the floodwave [m/d]
x_W	distance of a well location away from a stream [m]
Y	large section of stream used to evaluated total stream depletion [m]
β	$p + f_y^2$ [-]
δ	Dirac delta function [m^{-1}].

ω	frequency of the flood wave

Subscript *D* denotes dimensionless variable and parameter.

Overbar denotes variable in Laplace domain.

Double bar denotes variable in Fourier domain.

$'$ denote parameter in the streambed.

Subscript 1 denotes stream depletion caused by stream stage fluctuations

Subscript 2 denotes stream depletion caused by pumping

List of symbols for Chapter III

$\zeta(z)$	complex potential
ϕ	potential function
ψ	stream function
α_n	$\frac{1}{2}-\frac{1}{4\omega_n}\left[\sin\left(2\omega_n+2\mu_n\right)-\sin\left(2\mu_n\right)\right]$
β_1	K/K_1 [-]
β_2	K/K_2 [-]
ω_n	spatial frequency term
μ_n	phase term
H_n	$\frac{2\pi}{\alpha_n\omega_n}\sin\left(\omega_n a_D+\mu_n\right)\exp\left(-\omega_n\lvert y_D\rvert\right)$
a	location of the pumping well along x-axis [m]
B	aquifer thickness [m]

C_1	conductance of Streambed 1 or K_1/B_1 [d^{-1}]
C_2	conductance of Streambed 2 or K_2/B_2 [d^{-1}]
h	hydraulic head in the aquifer [m]
h_1	hydraulic head in Stream 1 [m]
h_2	hydraulic head in Stream 2 [m]
K	hydraulic conductivity of aquifer [m/d]
L	Distance between two streams or streambeds [m]
q	regional flow [m/d]
Q	pumping rate [m^3/d]
Q_{s1}	Total stream depletion of Stream 1 [m^3/d]
Q_{s2}	Total stream depletion of Stream 2 [m^3/d]
z	complex number

Subscript *D* denotes dimensionless variable and parameter

Subscript *c* denotes critical condition

Subscript 1 denotes parameter in Streambed 1 or Stream 1

Subscript 2 denotes parameter in Streambed 2 or Stream 2

TABLE OF CONTENTS

CHAPTER Page

LIST OF FIGURES

FIGURE Page

LIST OF TABLES

TABLE Page

CHAPTER I

INTRODUCTION: THE IMPORTANCE OF RESEARCH

Global water balance, which is significant to many applications such as climate models and chemical cycles, has many components such as evapotranspiration, precipitation, and groundwater. Some of the components can be measured or can be estimated in fairly straightforward fashions. For instance, river discharge into the ocean can be monitored at all time using stream gage and velocity measurement. However, some components are difficult to measure or to estimate, and such components often contribute significant errors to the global water balance. Stream aquifer interactions are one of these components. Better understanding stream aquifer interactions could significantly reduce the errors in the global water balance.

This dissertation focuses on stream depletion. Stream depletion is water flux flowing out of the stream or flux flowing into the stream, which usually occur at stream bank or at the bottom of stream channel. Figure 1.1 is a schematic cross-section of a stream-aquifer system without any streambed, and all symbols are described in the nomenclature on page vii. In this case, the stream is fully penetrating through the entire thickness of the confined aquifer. The bottom of the system is assumed to be no-flow boundary which could be a thick layer of clay or other low permeability materials. In this case, stream depletion only occurs at the stream bank. This model is valid in an area where water table or potentiometric surface is shallow, such as in the northeast of the

---

This dissertation follows the style of Journal of Hydrology.

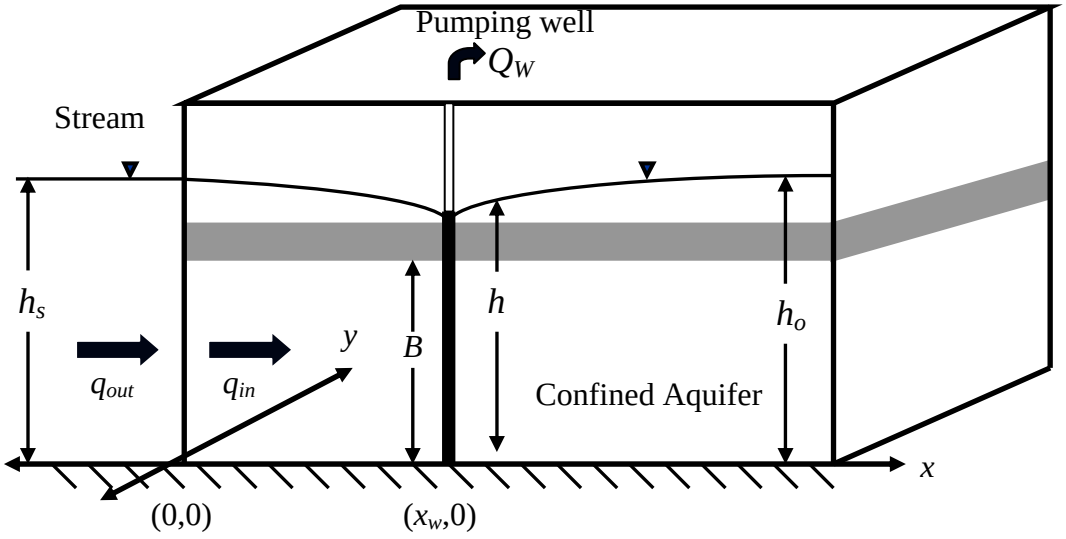

Figure 1.1 Schematic cross-section of fully penetrating stream-aquifer system without streambed.

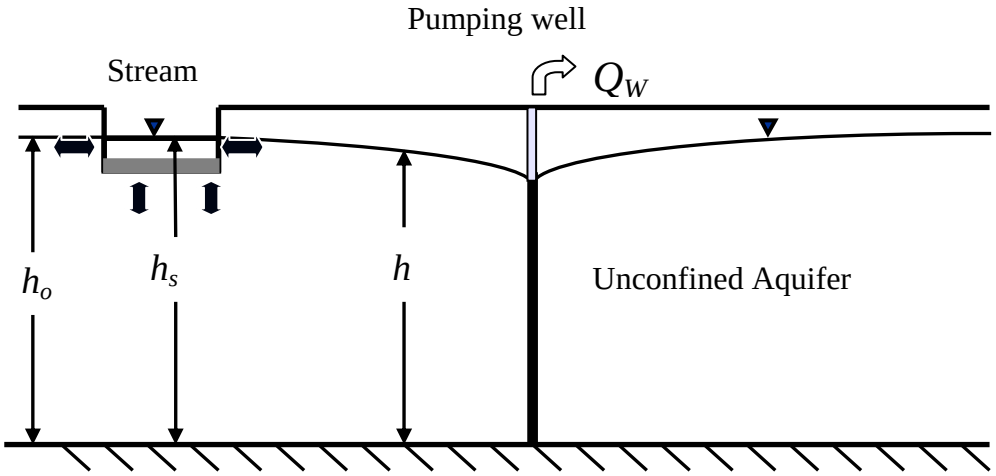

Figure 1.2 Schematic cross-section of partially penetrating stream-aquifer system with streambed.

United States.

Theis (1941) presented analytical solution of stream depletion caused by a fully penetrating pumping well in a homogeneous confined aquifer without streambed assuming that the stream stage is constant (Figure 1.1). Hantush (1965) added streambed at the stream bank to Theis' (1941) model and derived analytical solution of stream depletion. Zlotnik et al. (1999) and Butler et al. (2001) presented analytical solutions of stream depletion rate caused by a fully penetrating pumping well in a homogeneous unconfined aquifer near a partially penetrating pumping well with streambed at the bottom of the channel (Figure 1.2). In this case, stream depletion occurs at the stream bank and at the streambed. The black arrows indicated the areas where stream depletion occurs. This model is likely to valid in an area where water table is deep, such as the southwest of the United States. Hunt (1999) considered stream-aquifer system similar to Zlotnik et al. (1999) and Butler et al. (2001), except that the stream is infinitely small.

Stream aquifer interaction is complex and composes of fluxes caused by various factors such as stream stage fluctuations, evapotranspiration, and precipitation. Because the primary goal of this study is to provide a mean to quickly estimate stream depletion rate, analytical method is chosen. Assumptions made to simplify the problem are: first, stream depletion caused by stream stage fluctuation and a pumping well. Second, there is one layer of confined aquifer. Third, streambed and aquifer are homogeneous. Fourth, more assumptions are mentioned in section 2.2 on page 14.

In actual field conditions, there are many factors caused water movement between the stream and the aquifer such as regional flow and plants along the stream.

This study only considers stream depletion caused by stream stage fluctuation and a pumping well. If a pumping well is near a stream, the pumping well is often assumed to be the dominant cause of stream depletion. This study verifies this assumption and indicates when this assumption is likely to be violated by comparing the stream depletion rates caused by a pumping well and stream stage fluctuations. Depending on the setting, different factors neglected in this study can be important. For example, Loheide et al. (2005) showed that evapotranspiration can reduce up to approximately 20% of stream flow. If other components are significant, they can be superimposed to the solutions of this study.

Second, this study considers the stream-aquifer system with a fully penetrating well near a fully penetrating stream in Chapter II (Figure 2.1 and 2.2, page 16) and the stream-aquifer system with a fully penetrating well between two fully penetrating streams in Chapter III (Figure 3.1 and 3.2, page 59 and 62). In both chapters, the confined aquifer has one layer with no flow boundaries at the bottom of the system. In reality, the stream-aquifer system can be complex and can compose of multiple layers. If the system has multiple layers of aquifers and the hydraulic conductivities of the aquifers vary in different layers, the stream depletion rates in each layer would be various depending upon the hydraulic conductivities of the aquifers. However, the total stream depletion caused by stream stage fluctuations which is equal to sum of stream depletion from each layer, should be approximately equal to the depletion rate of the one-layer case.

Third, this study assumes that the streambed is a homogeneous layer of low conductivity sediment. However, streambed can be composed of multiple layers of sediment with various hydraulic conductivities and thicknesses. Because of the assumed geometry of the stream-aquifer system (Figure 2.2, page 16), the flow is always perpendicular to the streambed. The total hydraulic conductivity of the streambed is the average hydraulic conductivities of each layer.

One of the primary goals of this dissertation is to estimate and to compare the stream depletion caused by stream stage fluctuations and a pumping well. However, one should keep in mind that the real stream aquifer system is complex and that this study has many assumptions. Hence, one should treat the derived solutions of this study as a first approximation to understand the dynamics of the stream-aquifer system, rather than providing accurate solutions for realistic field situations.

This dissertation only considers water exchanges between the stream and the aquifer, but the results can be used as an input in other applications such as modeling chemical reactions near the stream-aquifer interface. Stream water typically has different chemical characteristics such as higher oxygen level than that of groundwater. When stream water migrates into the aquifer, chemical reactions such as oxidation, reduction, and precipitation can occur. Furthermore, groundwater often has anaerobic condition while the stream has aerobic condition. Adding oxygen-rich stream water to ground water could enrich oxygen near stream aquifer interface, and this can increase biological activity of microorganisms in the aquifer. These chemical and biological activities can

alter hydraulic properties of the aquifer. For example, mineral precipitation can clog pore space and can reduce hydraulic conductivity of the aquifer.

Increasing population leads to increasing water demands, and water shortage will become more severe and wide spread. The water shortage problem refers to a shortage of clean and low cost fresh water. Technology such as desalinization can provide abundance of clean fresh water at high cost which is not economically feasible for many uses such as aquiculture or industry. Induced stream depletion by a pumping well near a stream can obtain large quantities of cleaner water at a relatively low cost.

Groundwater is typically a cleaner source of water, but it is often a limited resource. Groundwater is naturally filtered by an aquifer and sediment; hence, it tends to have high quality. In addition, it is harder for groundwater to be contaminated because it is difficult for pollutants to migrate through layers of sediment to reach groundwater. Layers of sediments filtering groundwater also slow down its movement resulting in a longer replenishing period. The major limitation of groundwater as a water resource is its availability. Groundwater withdrawal rate is limited by groundwater recharge rate. However, groundwater withdrawals in many areas exceed groundwater recharges which could lead to problems such as subsidence and seawater intrusion. Another disadvantage of groundwater is its production cost is relatively higher than the cost of surface water, especially for areas that have deep aquifers. Higher production cost of groundwater is offset by lower treatment cost. Hence groundwater is a desirable source of water.

Surface water, on the other hand, is more abundant and easy to access, but it trends to be contaminated. The availability of surface water typically exceeds the

availability of groundwater. Surface water has a lower production cost; however, its treatment cost is often higher than the treatment cost of groundwater. Typically, it is more expensive to produce drinking water from surface water than from groundwater because of high treatment cost. Rain drops can absorb pollution in the atmosphere. Once rain drops reach the ground, they could be further contaminated. Surface water can also be contaminated in its reservoirs by human processes or natural processes such as algae blooms. Despite higher cost, cities are forced to use surface water as sources of water supplies.

Induced stream depletions by a pumping well near a stream can utilize the high availability of surface water and lower treatment cost of groundwater. At the beginning, extracted water from a pumping well near a stream or a lake comes from aquifer storage. As pumping continues, a cone of depression expands and reaches the stream. Then the majority or all of extracted water originates from the stream. Extracted water typically has higher quality than stream water because sediment between the well and the stream filtered turbidity and contaminants. This lowers the treatment cost which often exceeds the cost of pumping. Hence, induced stream depletions by a pumping well near a stream can become a significant water supply at a competitive price.

Induced stream depletions by a pumping well reduce stream flow rates, which can have significant impacts on hydrological and ecological systems. Induced stream depletion can impact the dynamic of gaining and losing streams which could lead to terrain alterations such as a change from a wetland to a grass field. A lower flow rate also impacts species in a habitat which can lead to extinction if those species cannot

adjust to the altered environment. To sustain the dynamic of the system, it is important to determine a pumping rate that yields minimum impacts on hydrological and ecological systems. The long-term goal of this study is to use these solutions combined with real time stream stage and other hydrological data to calculate maximum pumping rate, which allows sustainable stream flow rate to maintain ecological systems.

This dissertation presents two systems with a fully penetrating pumping well in a confined aquifer near a fully penetrating stream: one with streambed and one without, as is discussed in Chapter II. Two functions are used to represent stream stage fluctuations. For the seasonal case, stream stage is a function of time, and cosine of time is used as an example of seasonal stream stage fluctuation. For the short-term case, stream stage is a function of time and distance along a stream, and a Gaussian function is used as example of stream stage of a flood wave. Stream depletion rates in Chapter II are solved using the Laplace and Fourier methods. In Chapter III, stream-aquifer systems with a fully penetrating pumping well in a confined aquifer between two parallel fully penetrating streams with and without streambeds are discussed. For these cases, we assume that the stream stage is constant. Stream depletion rates in Chapter III are solved using the potential method. Capture zone analysis are also conducted for these cases.

CHAPTER II

ANALYTICAL AND SEMI-ANALYTICAL SEASONAL STREAM DEPLETION RATES CAUSED BY A PUMPING WELL NEAR A STREAM AND STREAM STAGE FLUCTUATIONS

Stream depletions caused by a pumping well near a stream are influenced by components which are the pumping rate and stream stage fluctuations. Previous studies often focus on each component separately. This study examines and compares two components together for various hydraulic settings and pumping schemes. This study presents generalized solutions for stream depletions in Laplace domain caused by a pumping well and caused by stream stage fluctuations with and without streambeds. It focuses on seasonal stream depletion rates with a time-dependent stream stage. The stream stage as a cosine function of time is chosen as a model for all scenarios. Three pumping schedules are 1) pumping for two months during a dry season with a maximum rate; 2) pumping for four months of the dry season with half of the maximum pumping rate; and 3) constant pumping through out a year with one sixth of the maximum rate. The maximum pumping rates of 1,000m^3/d is chosen to simulate an irrigation well or a municipal well. The primary characteristic of the hydrograph affecting stream depletion is its period. For the maximum pumping rate of 1,000 m^3/d and the period of one year, percentages of the maximum stream depletion rates caused by stream stage fluctuations to the maximum total stream depletion rate range from 7.6% to 31% for a stream reach of 1,000 m. Reducing the flood period to 30 days, the percentages then range from 29%

to 61%, increasing by approximately two or three times. The amplitude of the flood wave does not contribute significantly to depletion rates. Adding streambeds of 0.2m to 1m thick with its hydraulic conductivity of 1/1000 of the aquifer hydraulic conductivity, the percentages are approximately 3% to 16% smaller than ones without streambed. The late time approximation of the stream depletion rate caused by stream stage fluctuations is inversely proportional to the square root of time for a stream stage following the cosine fluctuation function; therefore, stream depletion caused by stream stage fluctuations after a sufficiently long time can be neglected.

2.1 Introduction

Hydrologists have been fascinated with the stream-aquifer interaction research for many decades for a number of reasons. Stream-aquifer interface is a critical zone where surface water and groundwater exchange mass, energy, and chemicals. For instance, base flow from an aquifer to the adjacent stream plays an important role for maintaining sustainable stream flow, particularly during the dry seasons. Discharge of groundwater with rather small temperature fluctuations to a stream is vital for maintaining sensitive ecological zones in the stream for fish reproduction and other biological processes. For many decades, groundwater withdrawal wells have been placed near streams to obtain high quality and plentiful water, a process that will result in stream depletion. Climate change caused by global warming will change the intensity and duration of precipitation, which affects the stream flow and eventually affect stream-aquifer interaction. Understanding the dynamics of stream-aquifer interaction is one of

the most important research topics for hydrologists. At present, studies of stream-aquifer interaction can be generally summarized into two types as type-A and type-B. The type-A studies focus on investigating the stream depletion caused by pumping wells, assuming that the stream stage does not change. The type-B studies focus on investigating the aquifer response to stream stage fluctuation without involving any pumping wells.

The type-A studies are briefly reviewed first. Theis (1941) and Jenkins (1968, 1970) presented analytical solutions of stream depletion for fully penetrating streams without streambeds into isotropic and homogeneous aquifers caused by nearby pumping wells with constant pumping rates. The highly simplified model of Theis (1941) and Jenkins (1968, 1970) were later improved by many investigators including Rorabaugh (1963), Hantush (1965), Wallace et al. (1990), Hunt (1999), Chen and Yin (2001), Zlotnik and Huang (1999), Butler et al. (2001), Kirk and Herbert (2002), and Sun and Zhan (2007). Among these investigations, Hantush's (1965) work was notable for its inclusion of semi-permeable streambeds adjacent to the stream, but it only considered a fully penetrating stream. Hunt (1999) tried to improve Hantush's (1965) model and provided analytical solutions of stream depletion by considering a narrow and shallow stream. However, as pointed out by Sun and Zhan (2007), Hunt's (1999) model was mathematically identical to that of Hantush (1965), provided that the Dupuit assumption was invoked. To address the issue of partial penetration of the stream, one has to consider vertical flow near the stream and cannot adopt the Dupuit assumption (Sun and Zhan, 2007). Several other investigators also studied the steady-state capture zones near

one or two streams when regional flow was presented (Newsom and Wilson, 1988; Intaraprasong and Zhan, 2007). Horizontal wells have also been proposed as alternative ways for withdrawing groundwater from aquifers near streams or underneath streams (Zhan and Park, 2003; Sun and Zhan, 2006). One of the advantages of using horizontal wells versus vertical wells is the theoretically unlimited screen lengths that can be used in horizontal wells to increase the interceptive volumes with groundwater.

Numerical simulations have also been carried out for the type-A studies. For example, Spalding and Khaleel (1991) compared Theis (1941) and Hantush's (1965) solutions against numerical models, and assessed the possible errors resulted from using simplified assumptions in the analytical solutions such as neglect of partial penetration, neglect of clogging layer resistance, and neglect of storage in areas beyond the stream. Sophocleous et al. (1995) compared stream depletion caused by a fully penetrating well near a fully penetrating stream with no streambed using the analytical solution of Theis (1941) and a numerical solution involving the STREAM module of MODFLOW (Prudic, 1989), and concluded that the differences between the analytical and numerical solutions ranged from 2% to 8%. Sophocleous et al. (1995) also compared Hantush's (1965) analytical solution to the numerical solution of stream depletion caused by a fully penetrating pumping well near a fully penetrating well with a clogging streambed, and reported significant discrepancies ranging from 58 to 71%.

There are also numerous type-B studies that concern aquifer response to stream stage changes. For example, Moench and Barlow (2000) and Barlow and Moench (1998) developed solutions for several cases of transient hydraulic interaction between a fully

penetrating stream and a confined, leaky, or water table aquifer to calculate aquifer heads, bank infiltration rates, and bank storage that occur in response to stream-stage fluctuations and basin-wide recharge or evapotranspiration. Hantush (2005) investigated channel flow and stream-aquifer interaction in response to impulse and step response functions of the streams, and associated flow volumes to hydrologic processes and regulatory and management control measures. Other examples of the recent type-B studies include Akylas and Koussis (2007), Kim et al. (2007), Sun and Zhan (2007), Singh (2004), and Chen and Chen (2003a).

In reality, groundwater withdrawal and stream stage fluctuation represent two different stimuli of the hydrological system and is likely to occur simultaneously. These two stimuli have rather different physical natures. For instance, a pumping well can be characterized as second-kind (Neumann) boundary condition, whereas the stream stage fluctuation belongs to a first-kind (Dirichlet) boundary condition. Therefore, it is not always clear how the hydrological system will response when both stimuli are functioning at the same time. For instance, the primary question that needs to be answered is: which stimuli, under what condition will dominate the stream depletion? By comparing groundwater withdrawal and stream stage fluctuation on stream depletion and other phenomena, one can understand the dynamics of stream-aquifer interaction in a better way which can help optimize groundwater withdrawal near a stream without causing detrimental effects. For example, by observing the trend of stream stage fluctuation, one can select the location of pumping wells and the adequate pumping rates and durations to better manage the stream-aquifer system. The goal of this study is to

investigate the stream-aquifer system considering both groundwater withdrawal and stream stage fluctuations. Although the solutions provided in this dissertation can be used for understanding a broad range of problems associated with stream-aquifer interaction, our focus is primarily on the stream depletion issue.

2.2 Model Descriptions

There are four basic conceptual models of a stream and aquifer system: 1) Theis (1941) model of a fully penetrating stream with a perfect hydraulic connection to an aquifer 2) Hantush's (1965) model of a fully penetrating stream with streambeds in an aquifer 3) Hunt's (1999) model of a partially penetrating and infinitesimal width stream with streambeds. 4) Zlotnik and Huang (1999) and Butler et al.'s (2001) model of a partially penetrating stream with a finite width and clogging streambeds. All models assume Dupuit approximation and that the aquifer is homogeneous and isotropic. As discussed in Sun and Zhan (2006), Hunt's (1999) solution is identical to that of Hantush (1965) for a fully penetrating stream. This is because one cannot distinguish the geometric difference of a partially penetrating stream from a fully penetrating stream under the Dupuit assumption. Such a geometric difference can only be exhibited under a three-dimensional view of flow. In addition, the models of partially penetrating streams with finite widths developed by Zlotnik and Huang (1999) and Butler et al. (2001) were found to be close to the mathematically simpler model of Hunt's solution (1999) under many practical circumstances. Given above consideration, we choose to examine stream

depletion caused by a fully penetrating well near a fully penetrating stream with and without clogging streambeds.

Figures 2.1 and 2.2 show the schematic cross-sectional diagrams of fully penetrating wells in homogeneous and confined aquifers near fully penetrating streams with and without clogging streambeds. The hydraulic conductivities of the streambeds are expected to be a few orders of magnitude smaller than those of the aquifers. One should be aware that realistic geological conditions of the stream-aquifer system could be much more complicated than what has been shown in Figures 2.1 and 2.2. For instance, the streambed could be a highly complex, heterogeneous, and often poorly defined zone that is difficult, if not impossible to be described using a single set of hydraulic parameters (Kollet and Zlotnik, 2003). The stream channel could meander around certain curves. Such complexities will be simplified in order to make the analytical study amendable. There is no question that such simplifications will introduce errors when one tries to apply the derived solutions for more complex, realistic situations. In this regard, one should treat the derived solutions of this study as a first approximation to understand the dynamics of the stream-aquifer system, rather than providing accurate solutions for realistic field situations. The derived solutions are probably more useful for gaining physical insights on the stream-aquifer system by varying several involved physical parameters and for testing numerical solutions. Nevertheless, the following assumptions are adopted.

First, the aquifer has a constant thickness and extended to infinity horizontally. Second, the streambed, if considered, is homogeneous with a constant thickness. Third,

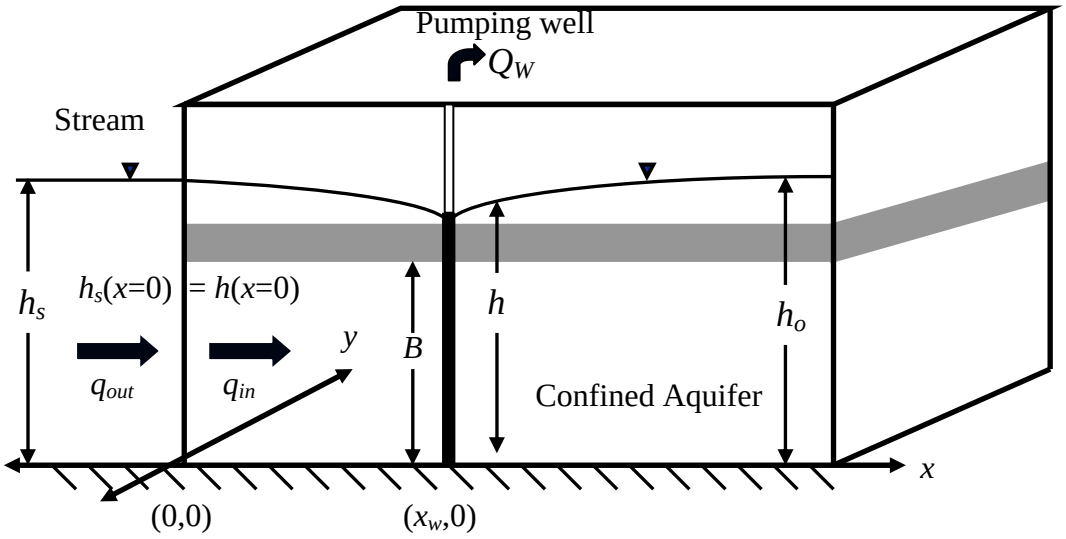

Figure 2.1 Schematic cross-section of stream-aquifer system without streambed.

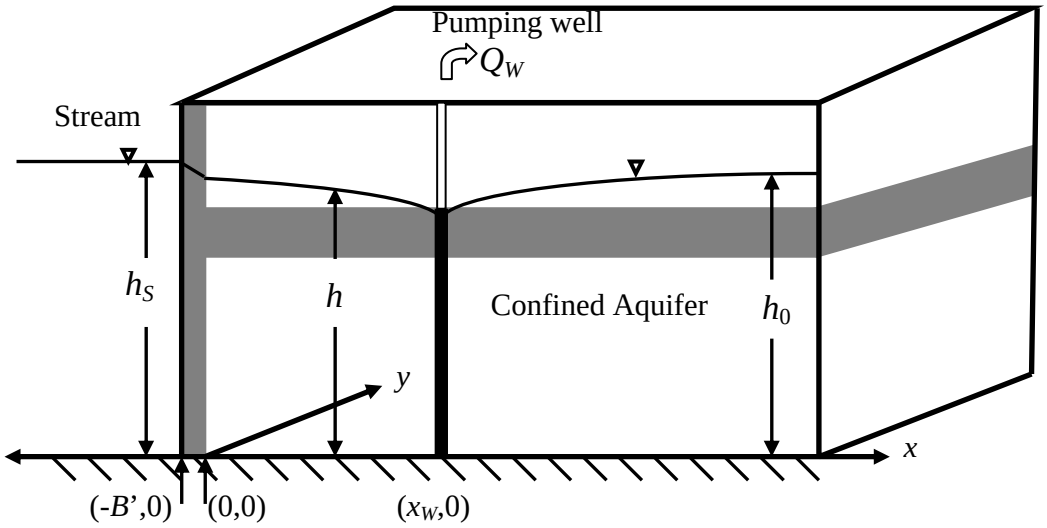

Figure 2.2 Schematic cross-section of stream-aquifer system with streambed.

the stream stage is always above or equal to the top elevation of the aquifer to ensure the confined condition of the aquifer. Fourth, regional flow (base flow) towards the stream is not considered, but can be directly superimposed on the solutions of this study. Fifth, the stream is assumed to be straight at the domain of interested. The *x*-axis is perpendicular to the stream and passes through the pumping well. The stream is along the *y*-axis. The origin is at the aquifer-stream boundary if streambed does not exist or at the streambed-aquifer boundary is streambed exists.

2.3 Mathematical Derivation without Low-permeability Streambed Sediment

2.3.1 Seasonal drawdown in the aquifer

The governing equation of groundwater flow in an aquifer described in Figure 2.1, together with the initial and boundary conditions at the stream are given as following

$$S_s \frac{\partial h}{\partial t} = K_x \frac{\partial^2 h}{\partial x^2} + K_y \frac{\partial^2 h}{\partial y^2} + \frac{Q_W(t)}{B}\delta(x - x_W)\delta(y), \tag{2.1}$$

$$h(x, y, t = 0) = h_0, \tag{2.2}$$

$$h(x = \infty, y, t) = h_0, \tag{2.3}$$

$$h(x = 0, y, t) = h_S(t), \tag{2.4}$$

where h is hydraulic head in the aquifer [L]; h_0 is initial hydraulic head in the aquifer and is a constant [L]; h_s is hydraulic head in the stream and is time-dependent [L]; K_x and K_y are the hydraulic conductivities of the aquifer along the x and y directions, respectively [L/T]; t is time [T]; Q_W is pumping rate of the well [L^3/T]; S_s is specific storage [L^{-1}]; B is aquifer thickness [L]; $\delta()$ is the Dirac delta function [L^{-1}]. (x_W, 0) is

the location of the pumping well. Defining drawdown in the aquifer, *s*, and drawdown in the stream, H_S, as: $s(x,y,t) = h_0 - h(x,y,t)$, and $H_S(t) = h_0 - h_S(t)$. Defining Laplace transform and inverse Laplace transform as:

$$\bar{s} = \int_{-\infty}^{\infty} s e^{-pt} dt, \qquad s = \frac{1}{2\pi i} \int_{c-i\infty}^{c+i\infty} \bar{s} e^{pt} dp,$$

where the overbar denotes variable in Laplace domain, *p* is Laplace transform parameter, $i = \sqrt{-1}$ is the complex sign, and *c* is a real number so that all the singularity points of $\bar{s}$ are on the right side of the integration path.

Defining Fourier transform and inverse Fourier transform along the *y*-axis as:

$$\bar{\bar{s}} = \int_{-\infty}^{\infty} \bar{s} e^{if_y y} dy, \qquad \bar{s} = \frac{1}{2\pi} \int_{-\infty}^{\infty} \bar{\bar{s}} e^{-if_y y} df_y,$$

where $\bar{\bar{s}}$ is the Fourier transform of $\bar{s}$, and f_y is the Fourier transform variable (spatial frequency). The associated dimensionless variables are defined in Table 2.1.

After converting Eqs. (2.1)-(2.4) to dimensionless forms and applying the Laplace-Fourier transforms, one will obtain the following solutions of drawdown.

$$\bar{\bar{s}}_D = \hat{\bar{H}}_{SD} e^{-\sqrt{\beta} x_D} + \frac{4\pi}{\sqrt{\beta}} \bar{Q}_{WD} e^{-\sqrt{\beta} x_{WD}} \sinh(\sqrt{\beta} x_D), \text{ for } 0 \le x_D \le x_{WD}, \tag{2.5}$$

$$\bar{\bar{s}}_D = \hat{\bar{H}}_{SD} e^{-\sqrt{\beta} x_D} + \frac{4\pi}{\sqrt{\beta}} \bar{Q}_{WD} \sinh(\sqrt{\beta} x_{WD}) e^{-\sqrt{\beta} x_D}, \text{ for } x_{WD} < x_D, \tag{2.6}$$

Table 2.1 Dimensionless parameters and variables used in Chapter II.

$B'_D = \frac{B'}{B}$	$h_{SD} = \frac{4\pi B\sqrt{K_x K_y}}{Q_0} h_S$
$H_{SD} = \frac{4\pi B\sqrt{K_x K_y}}{Q_0} H_S$	$q_D = \frac{q}{\frac{Q_{WD}}{4\pi B}\sqrt{\frac{K_x}{K_y}}}$
$Q_{TD} = \frac{Q_{TD}}{Q_0}$	$Q_{1D} = \frac{Q_{1D}}{Q_0}, Q_{2D} = \frac{Q_{2D}}{Q_0}$
$Q_{WD}(t_D) = \frac{Q_W(t)}{Q_0}$	$s_D = \frac{4\pi B\sqrt{K_x K_y}}{Q_0} s$
$s'_D = \frac{4\pi B\sqrt{K_x K_y}}{Q_0} s'$	$t_D = \frac{K_x}{B^2 S_s} t$
$v_D = \frac{BS_s}{K_x}\sqrt{\frac{K_y}{K_x}} v$	$x_D = \frac{x}{B}$
$y_D = \frac{y}{B}\sqrt{\frac{K_x}{K_y}}, Y_D = \frac{Y}{B}\sqrt{\frac{K_x}{K_y}}$	$\mu = \frac{K_x S'_s}{K' S_s} = \frac{C_1}{C_2}$
$\lambda = \frac{K'}{K_x}$	$\omega_D = \omega\frac{B^2 S_s}{K_x}$

where $\hat{\bar{H}}_{SD} = 2\pi\bar{H}_{SD}(p)\delta(f_y)$ and $\beta = p + f_y^2$, and x_{WD} is defined in the same way as x_D. Detailed derivations of $\bar{\bar{s}}_D$ are shown in Appendix A (page 97), and nomenclature describes symbols used in Chapter II of this dissertation (page vii).

Eqs. (2.5) and (2.6) describe drawdown in the aquifer in the Laplace-Fourier domain. To obtain drawdown in the spatial-time domain, one must carry out the inverse Laplace-Fourier transform of Eqs. (2.5) and (2.6). Notice that the first term on the right hand side of Eq. (2.5) or Eq.(2.6) only contains variables describing stream stage fluctuations. The second term on the right hand side of Eq. (2.5) or Eq. (2.6) only contains variables describing influence of the pumping well. This finding is important because it implies that in the Laplace-Fourier domain, the influences of the stream stage and the pumping well upon drawdown can be superimposed, although the stream stage is a first-kind (Dirichlet) boundary and the pumping well is a second-kind (Neumann) boundary. Theoretically speaking, one can carry any kind of computation and analysis on the basis of Eqs. (2.5) and (2.6), but in the following we will focus on the stream depletion discussion.

2.3.2 Seasonal stream depletion

Stream depletion per unit stream reach, q [L^2/T], can be described with the following equation:

$$q = -K_x B\left.\frac{\partial h}{\partial x}\right|_{x=0} = \frac{Q_0}{4\pi B}\sqrt{\frac{K_x}{K_y}}\left.\frac{\partial s_D}{\partial x_D}\right|_{x_D=0}, \text{ or } q_D = \frac{q}{\frac{Q_0}{4\pi B}\sqrt{\frac{K_x}{K_y}}} = \left.\frac{\partial s_D}{\partial x_D}\right|_{x_D=0}, \qquad (2.7)$$

where q_D is the dimensionless form of q. Conducting Laplace transform and Fourier transform of Eq. (2.8), the result is

$$\bar{\bar{q}}_D = \left.\frac{\partial \bar{\bar{s}}_D}{\partial x_D}\right|_{x_D=0} = -\sqrt{\beta}\,\hat{\bar{H}}_{SD} + 4\pi \bar{Q}_{WD} e^{-\sqrt{\beta} x_{WD}} . \qquad (2.8)$$

Conducting inverse Fourier transform of Eq. (2.8), the result is

$$\bar{q}_D = \bar{q}_{1D} + \bar{q}_{2D} = -\sqrt{p}\,\hat{\bar{H}}_{SD} + 4\pi F^{-1}\left(\bar{Q}_{WD} e^{-\sqrt{\beta} x_{WD}}\right), \qquad (2.9)$$

where $\bar{q}_{1D}$ and $\bar{q}_{2D}$ represent the first and second terms of Eq. (2.9), respectively, and F^{-1} stands for the inverse Fourier transform. The first term on the right hand side of Eq. (2.9) describes stream depletion per unit stream reach caused by stream stage fluctuations, and the second term describes stream depletion caused by the pumping well.

Total depletion along the entire stream, Q_T [L^3/T], is a sum of q over the entire stream reach. In addition, Q_T is a sum of two components: one part from the stream fluctuations, Q_1, and the other from pumping well, Q_2. Because one of the assumptions is that the stream extends to infinity, Q_1 would be infinity. In order to compare Q_1 with Q_2, we choose to evaluate q_1 over a large section of a stream, Y, which should be greater than a capture zone of the pumping well. First, we derive the dimensionless stream depletion caused by stream stage fluctuations over a stream reach Y, Q_{1D}.

$$Q_{1D} = \frac{Q_1}{Q_0} = \frac{q_1 Y}{Q_0} = \frac{1}{4\pi} q_{1D} Y_D = -\frac{1}{4\pi} L^{-1}\left(\sqrt{p}\,\hat{\bar{H}}_{SD}\right) Y_D , \qquad (2.10)$$

where Y_D is dimensionless Y, defined in the same fashion as y_D (Table 2.1, page 19) and L^{-1} stands for the inverse Laplace transform. The inverse Laplace transform of Eq. (2.10) is

$$\overline{Q}_{1D} = -\frac{1}{4\pi}\sqrt{p}\hat{\overline{H}}_{SD}Y_D . \tag{2.11}$$

Second, we derive the dimensionless stream depletion caused by pumping well, Q_{2D}.

$$Q_{2D} = \frac{Q_2}{Q_0} = -\frac{1}{4\pi}\int_{-\infty}^{\infty}\frac{\partial s_{2D}}{\partial x_D}dy_D\bigg|_{x_D=0}, \tag{2.12}$$

where s_{2D} is the second term on the right hand side of Eq. (2.5). Conducting Laplace transforms of Eqs. (2.11) and (2.12) and

substituting $\int_{-\infty}^{\infty}\bar{s}_{2D}dy_D = \bar{\bar{s}}_{2D}(f_y = 0) = \frac{4\pi}{\sqrt{p}}\overline{Q}_{WD}e^{-\sqrt{p}x_{WD}}\sinh(\sqrt{p}x_D)$, the dimensionless stream depletion along the entire stream caused by pumping well is

$$\overline{Q}_{2D} = \frac{1}{4\pi}\frac{4\pi}{\sqrt{p}}\overline{Q}_{WD}e^{-\sqrt{p}x_{WD}}\sqrt{p} = \overline{Q}_{WD}e^{-\sqrt{p}x_{WD}} . \tag{2.13}$$

Hence, the total dimensionless stream depletion in Laplace domain can be expressed as

$$\overline{Q}_{TD} = -\frac{1}{4\pi}\sqrt{p}\overline{H}_{SD}Y_D + \overline{Q}_{WD}e^{-\sqrt{p}x_{WD}} . \tag{2.14}$$

Eqs. (2.5), (2.6) and (2.14) show that drawdown and stream depletion rate can be written in two separated terms and can be solved independently. If one would like to add additional component, it can be done by superposition another term in the existing result.

2.3.3 Short-term drawdown in the aquifer

The difference between the seasonal case and an individual flood case is that the seasonal flood wave function is a function of time while the individual flood wave is a function of time and distance along a stream. For a short time scale, stream stage varies along the stream. For a long time scale, stream stage is assumed to be constant along the stream. In this section, $\overline{\overline{H}}_S$ is not equal to $\overline{H}_S$ because H_S depend upon *y*. $\hat{\overline{H}}_{SD}$ in Section 2.3.1 is replaced by $\overline{\overline{H}}_{SD}$ for the derivations of drawdown of individual flood case. The rest follows the same step as the derivation of drawdown for seasonal case.

$$\overline{\overline{s}}_D = \overline{\overline{H}}_{SD} e^{-\sqrt{\beta} x_D} + \frac{4\pi}{\sqrt{\beta}} \overline{Q}_{WD} e^{-\sqrt{\beta} x_{WD}} \sinh(\sqrt{\beta} x_D), \text{ for } 0 \le x_D \le x_{WD}. \tag{2.15}$$

$$\overline{\overline{s}}_D = \overline{\overline{H}}_{SD} e^{-\sqrt{\beta} x_D} + \frac{4\pi}{\sqrt{\beta}} \overline{Q}_{WD} \sinh(\sqrt{\beta} x_{WD}) e^{-\sqrt{\beta} x_D}, \text{ for } x_{WD} < x_D. \tag{2.16}$$

Although the Eqs. (2.15) and (2.16) are similar to Eqs. (2.5) and (2.6), solving Eqs. (2.15) and (2.16) are more difficult because one must take inverse Fourier transform of $\overline{\overline{H}}_{SD}$.

2.3.4 Short-term stream depletion

For the same reason as in Section 2.3.3, $\overline{H}_{SD}$ is replaced by $\overline{\overline{H}}_{SD}$ for the derivation of stream depletion rates.

$$\overline{Q}_{TD} = -\frac{1}{4\pi} \sqrt{p} \overline{\overline{H}}_{SD} + \overline{Q}_{WD} e^{-\sqrt{p} x_{WD}}. \tag{2.17}$$

2.4 Mathematical Derivation with Low-permeability Streambed Sediment

2.4.1. Seasonal drawdown in the aquifer

If a streambed exists, there are several different ways to deal with it. Hantush (1965) has used a simplified method to handle the streambed by neglecting the storativity of the streambed. Such a treatment will be a good approximation if the streambed is relatively thin and one's primary interest is the long-term quasi-steady state behavior. The problem investigated here, however has a different focus. It involves transient variation of the stream stages, and the transient drawdown and stream depletions. For such transient hydrologic processes, it is unclear if the storativity of the streambed can be neglected or not. Therefore, we prefer to keep the streambed storativity in the analysis. Such a treatment is in line with several other recent investigation of stream-aquifer interaction studies such as Sun and Zhan (2006, 2007).

In addition to the governing equation in the aquifer as described in section 2.3.1, the governing equation of flow in the streambed, together with the initial and boundary conditions are given as follows

$$S_s' \frac{\partial h'}{\partial t} = K' \frac{\partial^2 h'}{\partial x^2}, \tag{2.18}$$

$$h'(t=0) = h_0, \tag{2.19}$$

$$h'(x=-B')=h_s(t)\,, \tag{2.20}$$

$$K'\left.\frac{\partial h'}{\partial x}\right|_{x=0}=K_x\left.\frac{\partial h}{\partial x}\right|_{x=0}\,, h'(x=0)=h(x=0)\,, \tag{2.21}$$

where h', K', S_s', B' denote the hydraulic head, hydraulic conductivity, specific storage, and thickness of the streambed, respectively. The streambed and the aquifer have the same initial head. Eq. (2.21) indicates that head and flux perpendicular to the streambed-aquifer interface are continuous. Drawdown in the streambed is defined as $\tilde{s}=h_0-h'$. A few new dimensionless terms associated with the streambed are defined as follows:

$$\tilde{s}_D=\frac{4\pi B\sqrt{K_xK_y}}{Q_0}\tilde{s}\,, B_D'=\frac{B'}{B}\,,\ \lambda=\frac{K'}{K_x}\,,\ \mu=\frac{K_xS_s'}{K'S_s}=\frac{C_1}{C_2}\,, \tag{2.22}$$

where $C_1=K_x/S_s$ and $C_2=K'/S_s'$ are the hydraulic diffusivity of the aquifer and streambed, respectively.

After converting the governing equations as well as the initial and boundary conditions of the aquifer and streambed into dimensionless forms and applying the Laplace-Fourier transforms, one will obtain the following solutions of drawdown. Expressions for the dimensionless drawdown in the streambed in Laplace-Fourier domain is and expressions for the dimensionless drawdown in an aquifer in the Laplace-Fourier domain are

$$\bar{\bar{s}}'_D = \hat{\bar{H}}_{SD} \frac{-\sqrt{\beta}\sinh\left(\sqrt{\mu p}x_D\right)+\lambda\sqrt{\mu p}\cosh\left(\sqrt{\mu p}x_D\right)}{\sqrt{\beta}\sinh\left(\sqrt{\mu p}B'_D\right)+\lambda\sqrt{\mu p}\cosh\left(\sqrt{\mu p}B'_D\right)} + \frac{4\pi\bar{Q}_{WD}e^{-\sqrt{\beta}x_{WD}}\sinh\left(\sqrt{\mu p}(x_D+B'_D)\right)}{\sqrt{\beta}\sinh\left(\sqrt{\mu p}B'_D\right)+\lambda\sqrt{\mu p}\cosh\left(\sqrt{\mu p}B'_D\right)}, \text{ for } -B'_D \le x_D < 0, \quad (2.23)$$

$$\bar{\bar{s}}_D = \hat{\bar{H}}_{SD} \frac{\lambda\sqrt{\mu p}e^{-\sqrt{\beta}x_D}}{\sqrt{\beta}\sinh\left(\sqrt{\mu p}B'_D\right)+\lambda\sqrt{\mu p}\cosh\left(\sqrt{\mu p}B'_D\right)} + 4\pi\bar{Q}_{WD}e^{-\sqrt{\beta}x_{WD}} \frac{\sqrt{\beta}\cosh\left(\sqrt{\beta}x_D\right)\sinh\left(\sqrt{\mu p}B'_D\right)+\lambda\sqrt{\mu p}\sinh\left(\sqrt{\beta}x_D\right)\cosh\left(\sqrt{\mu p}B'_D\right)}{\sqrt{\beta}\left(\sqrt{\beta}\sinh\left(\sqrt{\mu p}B'_D\right)+\lambda\sqrt{\mu p}\cosh\left(\sqrt{\mu p}B'_D\right)\right)},$$

for $0 \le x_D \le x_{WD}$, and (2.24)

$$\bar{\bar{s}}_D = \hat{\bar{H}}_{SD} \frac{\lambda\sqrt{\mu p}e^{-\sqrt{\beta}x_D}}{\sqrt{\beta}\sinh\left(\sqrt{\mu p}B'_D\right)+\lambda\sqrt{\mu p}\cosh\left(\sqrt{\mu p}B'_D\right)} + 4\pi\bar{Q}_{WD}e^{-\sqrt{\beta}x_D} \frac{\sqrt{\beta}\cosh\left(\sqrt{\beta}x_{WD}\right)\sinh\left(\sqrt{\mu p}B'_D\right)+\lambda\sqrt{\mu p}\sinh\left(\sqrt{\beta}x_{WD}\right)\cosh\left(\sqrt{\mu p}B'_D\right)}{\sqrt{\beta}\left(\sqrt{\beta}\sinh\left(\sqrt{\mu p}B'_D\right)+\lambda\sqrt{\mu p}\cosh\left(\sqrt{\mu p}B'_D\right)\right)},$$

(2.25)

for $x_{WD} < x_D$. Detailed derivations of $\bar{\bar{s}}_D$ and $\bar{\bar{s}}'_D$ are shown in Appendix B (page 99).

2.4.2 Seasonal stream depletion

Taking the same approach as the case without streambed, stream depletion per unit stream width, q [L^2/T], can be described with the following equation.

$$q = -K'_x B\left.\frac{\partial h'}{\partial x}\right|_{x=-B'} = \frac{Q_0 K'}{4\pi B}\sqrt{\frac{K_x}{K_y}}\left.\frac{\partial s'_D}{\partial x_D}\right|_{x_D=-B'_D}, \text{ or } q_D = \frac{q}{\frac{Q_0}{4\pi B}\sqrt{\frac{K_x}{K_y}}} = \lambda\left.\frac{\partial s'_D}{\partial x_D}\right|_{x_D=-B'_D}. \quad (2.26)$$

Conducting the Laplace-Fourier transform of Eq. (2.26), the result is

$$\overline{q}_D = \lambda\hat{\overline{H}}_{SD}\frac{-\sqrt{\beta\mu p}\cosh\left(\sqrt{\mu p}B'_D\right)-\lambda\mu p\sinh\left(\sqrt{\mu p}B'_D\right)}{\sqrt{\beta}\sinh\left(\sqrt{\mu p}B'_D\right)+\lambda\sqrt{\mu p}\cosh\left(\sqrt{\mu p}B'_D\right)}$$
$$+\lambda\frac{4\pi\overline{Q}_{WD}\sqrt{\mu p}e^{-\sqrt{\beta}x_{WD}}}{\sqrt{\beta}\sinh\left(\sqrt{\mu p}B'_D\right)+\lambda\sqrt{\mu p}\cosh\left(\sqrt{\mu p}B'_D\right)}. \quad (2.27)$$

Conducting the inverse Fourier transform of Eq. (2.27) leads to

$$\overline{q}_D = \overline{q}_{1D}+\overline{q}_{2D} = \lambda\hat{\overline{H}}_{SD}\frac{-\sqrt{\mu p}\cosh\left(\sqrt{\mu p}B'_D\right)-\lambda\mu\sqrt{p}\sinh\left(\sqrt{\mu p}B'_D\right)}{\sinh\left(\sqrt{\mu p}B'_D\right)+\lambda\sqrt{\mu}\cosh\left(\sqrt{\mu p}B'_D\right)}$$

$$+F^{-1}\left(\lambda\frac{4\pi\overline{Q}_{WD}\sqrt{\mu p}e^{-\sqrt{p}x_{WD}}}{\sqrt{\beta}\sinh\left(\sqrt{\mu p}B'_D\right)+\lambda\sqrt{\mu p}\cosh\left(\sqrt{\mu p}B'_D\right)}\right), \quad (2.28)$$

where $\overline{q}_{1D}$ and $\overline{q}_{2D}$ represent the first and second terms of Eq. (2.28), respectively and F^{-1} stands for the inverse Fourier transform. Identical to that of section 2.3.2, the first term on the right hand side of Eq. (2.28) describes stream depletion per unit stream reach caused by stream stage fluctuations, and the second term describes stream depletion caused by the pumping well. Using the same argument and steps as the case without streambed, one obtains the dimensionless stream depletion caused by stream stage fluctuation over a stream reach *Y*, Q_{1D} as

$$\overline{Q}_{1D} = -\frac{Y_D\lambda\hat{\overline{H}}_{SD}}{4\pi}\frac{\sqrt{\mu}\,p\cosh\left(\sqrt{\mu p}B'_D\right)+\lambda\mu p\sinh\left(\sqrt{\mu p}B'_D\right)}{\sqrt{p}\sinh\left(\sqrt{\mu p}B'_D\right)+\lambda\sqrt{\mu p}\cosh\left(\sqrt{\mu p}B'_D\right)}. \quad (2.29)$$

The dimensionless stream depletion caused by the pumping well, Q_{2D}, is defined as:

$$Q_{2D} = \frac{Q_2}{Q_o} = \frac{\lambda}{4\pi}\int_{-\infty}^{\infty}\left.\frac{\partial s'_{2D}}{\partial x_D}\right|_{x_D=-B'_D} dy_D, \quad (2.30)$$

where s'_{2D} is the second term on the right hand side of Eq. (2.23). The Laplace transform of Q_{2D} is

$$\overline{Q}_{2D} = \frac{\lambda}{4\pi}\left(\int_{-\infty}^{\infty} \frac{\partial \overline{s}'_{2D}}{\partial x_D} dy_D \right)\Bigg|_{x_D = -B'_D}, \tag{2.31}$$

where $\overline{s}'_{2D}$ is the Laplace transform of s'_{2D}. From Eq. (2.23), one gets

$$\int_{-\infty}^{\infty} \frac{\partial \overline{s}'_{2D}}{\partial x_D} dy_D = \overline{\overline{s}}'_{2D}(f_y = 0) = \frac{4\pi \overline{Q}_D e^{-\sqrt{p}x_{WD}} \sinh\left(\sqrt{\mu p}(x_D + B'_D)\right)}{\sqrt{p}\sinh\left(\sqrt{\mu p}B'_D\right) + \lambda\sqrt{\mu p}\cosh\left(\sqrt{\mu p}B'_D\right)}. \tag{2.32}$$

Substituting Eq. (2.32) in to Eq. (2.31), one has an expression for the dimensionless stream depletion caused by a pumping well.

$$\overline{Q}_{2D} = \frac{\lambda \overline{Q}_D \sqrt{\mu p} e^{-\sqrt{p}x_{WD}}}{\sqrt{p}\sinh\left(\sqrt{\mu p}B'_D\right) + \lambda\sqrt{\mu p}\cosh\left(\sqrt{\mu p}B'_D\right)}. \tag{2.33}$$

The dimensionless total stream depletion in Laplace domain expresses as following:

$$\begin{aligned} \overline{Q}_{TD} = & -\frac{Y_D}{4\pi}\lambda \hat{\overline{H}}_{SD} \frac{\sqrt{\mu p}\cosh\left(\sqrt{\mu p}B'_D\right) + \lambda\mu\sqrt{p}\sinh\left(\sqrt{\mu p}B'_D\right)}{\sinh\left(\sqrt{\mu p}B'_D\right) + \lambda\sqrt{\mu}\cosh\left(\sqrt{\mu p}B'_D\right)} \\ & + \frac{\lambda \overline{Q}_D \sqrt{\mu p} e^{-\sqrt{p}x_{WD}}}{\sqrt{p}\sinh\left(\sqrt{\mu p}B'_D\right) + \lambda\sqrt{\mu p}\cosh\left(\sqrt{\mu p}B'_D\right)} \end{aligned}. \tag{2.34}$$

2.4.3 Short-term drawdown in the aquifer

This section deals with a floodwave that is a function of time and distance along the stream, denoted as short-term stream flood. Similar to section 2.3.2, $\hat{\overline{H}}_{SD}$ in Section

2.4.1 is replaced by $\overline{\overline{H}}_{SD}$ for the derivations of drawdown of an individual flood case. The rest follows the same step as the derivation of drawdown for the seasonal case.

$$\bar{\bar{s}}'_D = \overline{\overline{H}}_{SD} \frac{-\sqrt{\beta}\sinh\left(\sqrt{\mu p}x_D\right)+\lambda\sqrt{\mu p}\cosh\left(\sqrt{\mu p}x_D\right)}{\sqrt{\beta}\sinh\left(\sqrt{\mu p}B'_D\right)+\lambda\sqrt{\mu p}\cosh\left(\sqrt{\mu p}B'_D\right)} + \frac{4\pi\overline{Q}_{WD}e^{-\sqrt{\beta}x_{WD}}\sinh\left(\sqrt{\mu p}(x_D+B'_D)\right)}{\sqrt{\beta}\sinh\left(\sqrt{\mu p}B'_D\right)+\lambda\sqrt{\mu p}\cosh\left(\sqrt{\mu p}B'_D\right)}, \text{ for } -B'_D \le x_D < 0, \tag{2.35}$$

$$\bar{\bar{s}}_D = \overline{\overline{H}}_{SD} \frac{\lambda\sqrt{\mu p}e^{-\sqrt{\beta}x_D}}{\sqrt{\beta}\sinh\left(\sqrt{\mu p}B'_D\right)+\lambda\sqrt{\mu p}\cosh\left(\sqrt{\mu p}B'_D\right)} + 4\pi\overline{Q}_{WD}e^{-\sqrt{\beta}x_{WD}} \frac{\sqrt{\beta}\cosh\left(\sqrt{\beta}x_D\right)\sinh\left(\sqrt{\mu p}B'_D\right)+\lambda\sqrt{\mu p}\sinh\left(\sqrt{\beta}x_D\right)\cosh\left(\sqrt{\mu p}B'_D\right)}{\sqrt{\beta}\left(\sqrt{\beta}\sinh\left(\sqrt{\mu p}B'_D\right)+\lambda\sqrt{\mu p}\cosh\left(\sqrt{\mu p}B'_D\right)\right)},$$

for $0 \le x_D \le x_{WD}$, and (2.36)

$$\bar{\bar{s}}_D = \overline{\overline{H}}_{SD} \frac{\lambda\sqrt{\mu p}e^{-\sqrt{\beta}x_D}}{\sqrt{\beta}\sinh\left(\sqrt{\mu p}B'_D\right)+\lambda\sqrt{\mu p}\cosh\left(\sqrt{\mu p}B'_D\right)} + 4\pi\overline{Q}_{WD}e^{-\sqrt{\beta}x_D} \frac{\sqrt{\beta}\cosh\left(\sqrt{\beta}x_{WD}\right)\sinh\left(\sqrt{\mu p}B'_D\right)+\lambda\sqrt{\mu p}\sinh\left(\sqrt{\beta}x_{WD}\right)\cosh\left(\sqrt{\mu p}B'_D\right)}{\sqrt{\beta}\left(\sqrt{\beta}\sinh\left(\sqrt{\mu p}B'_D\right)+\lambda\sqrt{\mu p}\cosh\left(\sqrt{\mu p}B'_D\right)\right)},$$

for $x_{WD} < x_D$. (2.37)

2.4.4 Short-term stream depletion

For the same reason as in Section 2.3.3, $\overline{H}_{SD}$ is replaced by $\overline{\overline{H}}_{SD}$ for the derivation of stream depletion rates.

$$\overline{Q}_{TD} = -\frac{\lambda}{4\pi}\overline{\overline{H}}_{SD}(f_y = 0)\left(\frac{-\lambda\mu\sqrt{p}\sinh\left(\sqrt{\mu p}B'_D\right)+\sqrt{\mu p}\cosh\left(\sqrt{\mu p}B'_D\right)}{\sinh\left(\sqrt{\mu p}B'_D\right)+\lambda\sqrt{\mu}\cosh\left(\sqrt{\mu p}B'_D\right)}\right) + \frac{\lambda\overline{Q}_{WD}\sqrt{\mu p}e^{-\sqrt{p}x_{WD}}}{\sqrt{p}\sinh\left(\sqrt{\mu p}B'_D\right)+\lambda\sqrt{\mu p}\cosh\left(\sqrt{\mu p}B'_D\right)} \quad . \tag{2.38}$$

2.5 Results and Discussion

2.5.1 Seasonal stream depletion without streambed

To obtain results, functions describing stream stages and pumping rates must be specified. As an example, we consider a hypothetic case in which a farm requires water during four months of the dry season and the owner of the farm decides to withdraw groundwater near a stream to meet the need. There are several different scenarios to design the annual pumping schedule, given the total amount of water the owner is permitted to pump. For the first scenario, the well is pumped at a constant rate of Q_0 during 2 months of the dry season per year. For the second scenario, the well is pumped at a rate of $Q_0/2$ for four months of the dry season per year. For the third scenario, the well is pumped at a rate of Q_0 /6 through out the entire year. This scenario intends to simulate a small municipal well or a small well that provide the farmer water for daily uses.

For the first scenario, assuming the pump is turned on at time t_0 with a rate of Q_0 until to t_s when it is shut down. Now one has to select the adequate stream stage fluctuation function. Most stream stage fluctuation could be complicated enough to be described by any mathematical functions. Rutschmann and Hager (1996) have discussed in details about various flood waves for different stream cross-sectional shape. One

possible way to handle the stream stage fluctuation is to numerically discritize the time domain into many small time intervals with piecewise step functions. The Laplace transform of such piecewise step functions can then be carried out numerically. This study, however, will not carry such a numerical calculation. Instead, we will pursue a simplified stream stage fluctuation function. Considering the fact that a seasonal variation trend is often observed from the hydrographs of many streams, therefore, it is possible to capture those seasonal changes via mathematical functions that are simple enough to be handled analytically. The following is a proposed stream stage function:

$$h_S(t) = A\left(1-\cos(\omega t)\right), \tag{2.39}$$

where A is the amplitude of the average hydrograph, and ω is frequency of the hydrograph. Eq. (2.39) is a simple enough function that has captured the seasonal variation of the hydrograph. It can be regarded as the first term of the Fourier series of the realistic hydrograph in time domain. Because of its simplicity, this equation has been used by many investigators such as Cooper and Rorabaugh (1963) and Singh (2004).

$H_S = h_0 - h_s = -A(1-\cos(\omega t))$, where $h_0 = 0$, and the dimensionless H_S is

$$H_{SD} = -\frac{4\pi AB\sqrt{K_x K_y}}{Q_0}(1-\cos(\omega_D t_D) = -C(1-\cos(\omega_D t_D), \tag{2.40}$$

where $C = \dfrac{4\pi AB\sqrt{K_x K_y}}{Q_0}$ and $\omega_D = \omega\dfrac{B^2 S_s}{K_x}$. Figure 2.3 shows the dimensionless stream stage, H_{SD}, and the dimensionless pumping rate, Q_{WD}, for all three scenarios with the parameters listed in Table 2.2. The chosen Q_0 of 1,000m^3/d is commonly seen for irrigation wells or water supply wells for small communities, and ω of $2\pi/360$ d^{-1} is

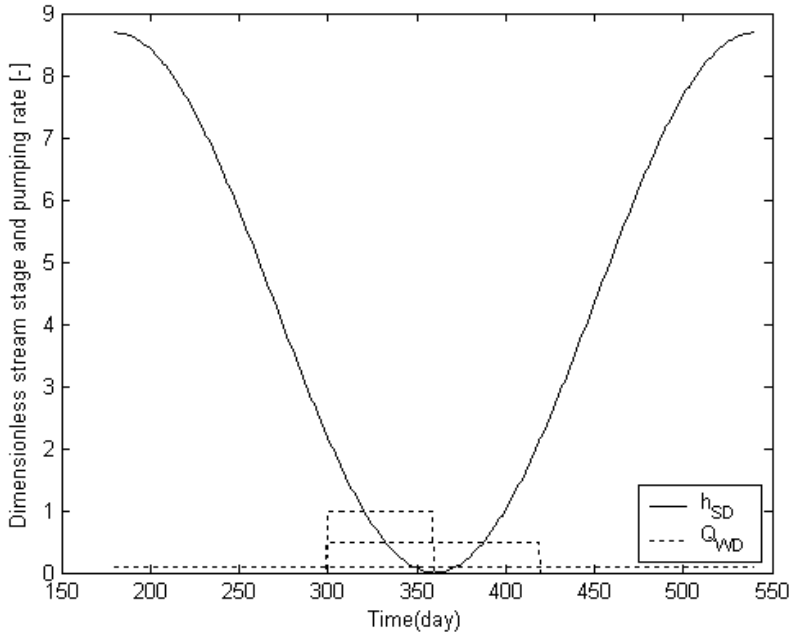

Figure 2.3 Dimensionless stream stage, h_{SD}, and dimensionless pumping rate, Q_{WD}, for all three scenarios with Q_0 of 1,000m^3/d with ω of $2\pi/360$ d^{-1}

Table 2.2 Hydraulic parameters used in Chapter II.

A = 2 m, A_0 = 1.5x10^5 m^2	B = 20 m	B' = 0.20 m and 1 m
D = 4x10^5 m^2/d	K_x = 8.63 m/d	K_y = 8.63 m/d
K' = 0.0086 m/d	Q_W = 1,000 m^3/d	S_s' = 0.0005 m^{-1}
S_s = 0.00005 m^{-1}	t_0= 300 d	t_s = 360 d and 420 d
v = 8x10^2 m/d	x_W = 50 m	$\omega = 2\pi/30$ d^{-1} , $2\pi/360$ d^{-1}

simulating annual hydrograph cycle. For pumping period of 2 and 4 months, pumping starts after 300 day, t_0, which is approaching the trough of the hydrograph. This signifies the day when the farmer plants seeds at the beginning of the summer, and crops requires irrigation until the day when the farmer stops pumping, t_s is at 420 d, which signifies the harvest or the beginning of rainy season when irrigation is no longer required. All results in section 2.5 only show one period of the hydrograph, excluding the beginning. Other hydrologic properties chosen to simulate a typical sandy aquifer are listed in Table 2.1 (page 19).

Applying the Laplace transform to Eq. (2.40) and substituting them into Eq. (2.14), the total dimensionless stream depletion for the case without streambed is

$$\overline{Q}_{TD} = \frac{CY_D}{4\pi}\left(\frac{\omega_D^2}{\sqrt{p}\left(p^2+\omega_D^2\right)}\right) + (e^{-t_{0D}p} - e^{-t_{sD}p})e^{-\sqrt{p}x_{WD}} \,. \qquad (2.41)$$

The first term on the right side of Eq. (2.41) represents the stream depletion caused by stream stage fluctuation in the Laplace domain. This term is the same as Cooper and Rorabaugh's (1963) solution in Laplace domain multiplied by Y_D after minor parameter conversion. This term in the real time domain can be numerically solved using the inverse Laplace transform of de Hoog et al. (1982), which was subsequently put into a Matlab program by Hollenbeck (1998). Theis (1941) solution for stream depletion caused by a pumping well with a constant pumping rate is $q/Q_0 = erfc\left(\frac{1}{2\tau}\right)$, where $\tau = (1/x_W)\sqrt{tK_x/S_s}$. The Theis' (1941) solution is for continuous groundwater withdrawal thus can be directly used for the third scenario. Superposition of Theis'

(1941) solution is used to obtain stream depletion caused by a pumping well for the first and the second scenarios. Since the pumping rate sharply changes at t_0 and t_s (Figure 2.3), analytical solutions provides more accurate results near these points than numerical solutions.

Figure 2.4 shows Q_{1D} and Q_{2Dj}, where the subscript j refers to number of months of pumping for a river reach, Y, of 1,000m. The chosen value of Y is 20 times the distance between the pumping well and the closest stream (x_W), and the rest of parameters have the same values as those used in Figure 2.3. The shape of Q_{1D} mimics the shape of the stream stage. Q_{1D} is small comparing to Q_{2D} in two, four, and twelve month extraction period cases. The maximum value of dimensionless stream depletion caused by stream stage fluctuations, $Q_{1D\max}$, is 0.074 when stream stage is near its peak. The dimensionless total stream depletion is denoted as Q_{TDj} where j is the months of pumping per year. The maximum value of Q_{TDj} for j=2 ($Q_{TD2\max}$) is 0.965, for j=4 ($Q_{TD4\max}$) is 0.522, and for j=12 ($Q_{TD12\max}$) is 0.239. Defining percentages of $Q_{1D\max}$ to $Q_{TDj\max}$ as $100Q_{1D\max}/Q_{TDj\max}$, then the percentages of $Q_{1D\max}$ to $Q_{TDj\max}$ for pumping periods of 2, 4 and 12 months are 7.64, 14.1, and 30.8% respectively. This comparison indicates that stream depletion is dominated by the pumping well for this case because of the relatively large pumping rate used here. Figure 2.5 shows the dimensionless total stream depletion rates, Q_{TDj}. For two and four months of groundwater extraction, Q_{TD} is almost identical to Q_{2D} because Q_{1D} is small comparing to Q_{2D} for the relatively large pumping rate. For all scenarios, Q_{TDj} are noticeably different from Q_{2D}. Q_{TD12} has the

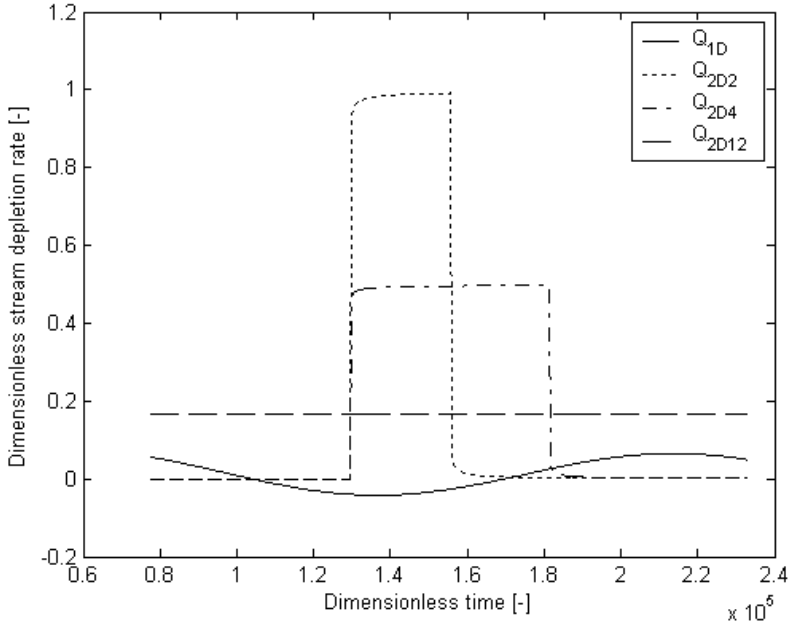

Figure 2.4 Dimensionless stream depletion rate caused by stream stage fluctuations, Q_{1D}, and caused by pumping well, Q_{2Dj}, where subscript j refers to number of months of pumping for Q_0 of 1,000m^3/d and ω of $2\pi/360$ d^{-1}.

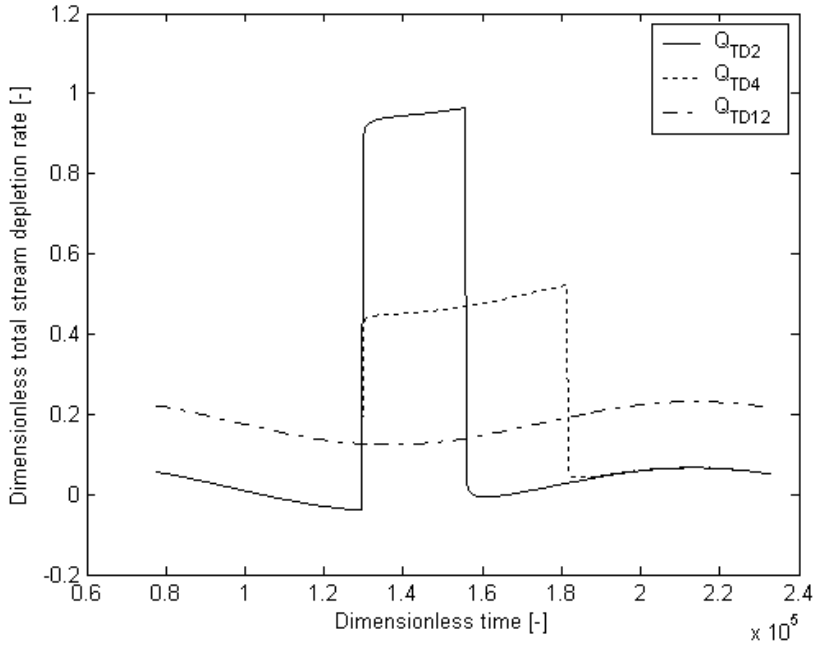

Figure 2.5 Dimensionless total stream depletion rate, Q_{TDj}, with Q_0 of 1,000m^3/d and ω of $2\pi/360$ d^{-1}.

same shape as Q_{1D}, but Q_{TD2} and Q_{TD4} have slightly decrease during pumping period comparing to its Q_{2D}.

The primary advantage of using dimensionless form is that the same result can be used to analyze many scenarios. For example in Chapter III, $Q_D = \frac{Q}{2\pi BLq}$, where Q is the pumping or injection rate (positive for pumping and negative for injecting), B is the aquifer thickness, L is distance between two streams, and q is regional flow rate. A system with Q of 1000 m^3/d, B of 20 m, L of 50 m, and q of 1 m/d and another system with Q of 1000 m^3/d, B of 10 m, L of 100 m, and q of 1 m/d would both yield the same value Q_D of $1/2\pi$. In Chapter II, stream depletion rate is normalized by Q_0 (Table 2.1 on page 19), this allows easy comparison between stream depletion caused by the pumping well and stream fluctuations. Using total volume of extracted water may be more useful in water management application, but the total volumes of extracted water are different for different maximum pumping rates, which makes it difficult to compare with other cases. The next paragraph will show the result of the same case discussed in the previous paragraph, but in total volume of extracted water as an example to calculate extracted volumes.

The total volume of extracted water from the well, V_T, is a sum of the pumping rate during the pumping period. The volume of extracted water caused by stream fluctuations, V_1, is sum of Q_1 during its pumping period. Similarly, the volume of extracted water caused by the pumping well, V_2, is Q_2 during its pumping period. V_T from three different pumping scenarios has the same value of 60000 m^3. V_1 are

approximately -2400, -2300, and 4600 m^3 for scenario 1, 2, and 3 respectively. The negative value indicates flow from aquifer into stream. V_2 are approximately 59000, 59300, and 59400 m^3 for scenario 1, 2, and 3 respectively. Sum of V_1 and V_2 are approximately 56700, 56900, and 64500 m^3 for scenario 1, 2, and 3 respectively. From a water management point of view, presenting these results in volume may be useful. However, it is difficult to compare the volume of extracted water from different scenarios. For example, the sum of V_1 and V_2 for pumping period of 2 months is different from that for pumping period of 12 months. The volumes of stream depletion caused by pumping are approximately equal for scenario 1 and 3, but the volumes of stream depletion caused by stream fluctuations of scenario 1 and 3 are different. For scenario 1, pumping begins and ends during dry season when groundwater flow into stream; therefore, V_1 of scenario 1 has negative value. V_1 of scenario 2 has a positive value because of the initial conditions. Comparing a ratio of V_1 or V_2 to the sum of V_1 and V_2 could be misleading because the sums of V_1 and V_2 have different values for different scenarios. Hence, the dimensionless stream depletion rate will be reported in the rest of Chapter II for easy comparison among different settings.

Three primary factors affecting Q_{1D} are Q_{WD}, ω_D, and Y_D. A higher pumping rate results in a higher Q_2 and a relatively lower Q_{1D} caused by scaling. Another primary factor affecting Q_{1D} is frequency of the hydrograph. Even though a difference between the crest of the stream stage and its trough is 4 m, slow changing of stream stage allowed the aquifer to response to the stream stage fluctuation. It takes approximately 180 days for stream stage to change from its peak to its trough. Hence a gradient between stream

stage and the aquifer is relatively small comparing to the gradient caused by the pumping well. To verify this hypothesis, we calculate these maximum values for ω = $2\pi/30$ d^{-1} and pumping periods of 5, 10, and 30 d. Figure 2.6 shows h_{SD}, and Q_{WD} for three pumping scenarios of 5, 10 and 30 d with the following values of parameters: ω of $2\pi/30$ d^{-1}, and the rest of the parameters are the same as ones used in Figure 2.3 (page 32). Figure 2.7 shows Q_{1D}, and Q_{2Dj}, where the subscript *j* refers to the number of days of pumping schemes. The general shape of this figure is the same as that shown in Figure 2.4 (page 34); however, one can notice a larger amplitude of Q_{1D} comparing to Q_{1D} in Figure 2.4. $Q_{1D\max}$ is 0.255, $Q_{TD2\max}$ is 0.877, $Q_{TD4\max}$ is 0.578, and $Q_{TD12\max}$ is 0.419. Percentages of $Q_{1D\max}$ to $Q_{TDj\max}$ for pumping periods of 5, 10 and 30 d are 29.1, 44.2, and 61%, respectively. Increasing the pumping frequency by a factor of six, percentages of $Q_{1D\max}$ to $Q_{TDj\max}$ for pumping periods of 5, 10 and 30 d increase by factors of 3.8, 3.1, and 2 comparing to percentages of $Q_{1D\max}$ to $Q_{TDj\max}$ for pumping periods of 2, 4 and 12 months respectively. These greater values show that a shorter wave period will lead to increased Q_{1D}. Figure 2.8 shows Q_{TDj}, where the subscript *j* refers to number of days of pumping with ω of $2\pi/30$ d^{-1}.

The amplitude of the hydrograph does not contribute significantly to Q_1. Using the amplitudes of 2m, 4m, and 6 m with the maximum pumping rate of 1,000 m^3/d, the Q_1 shows the nearly identical values for three amplitudes for the flood period of one year.

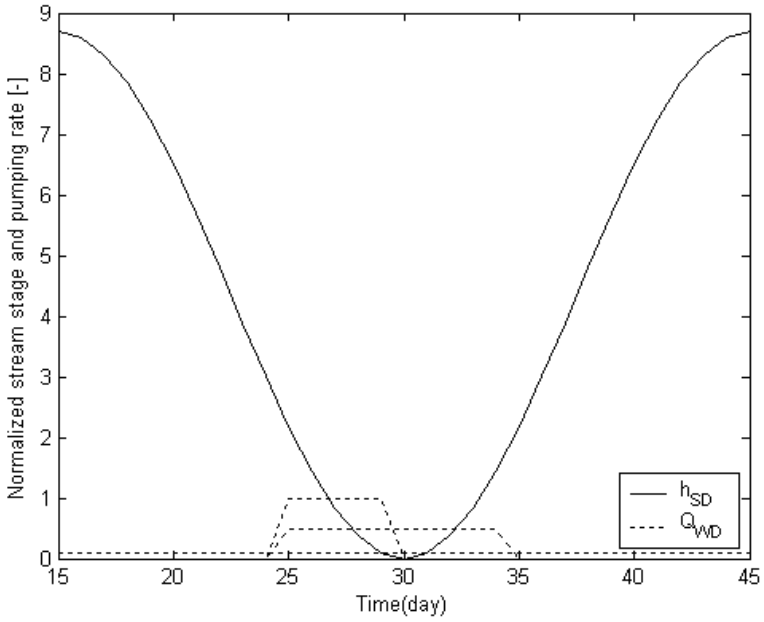

Figure 2.6 h_{SD} and Q_{WD}, for three pumping scenarios of 5, 10 and 30 d with Q_0 of 1,000m^3/d and ω of $2\pi/30$ d^{-1}.

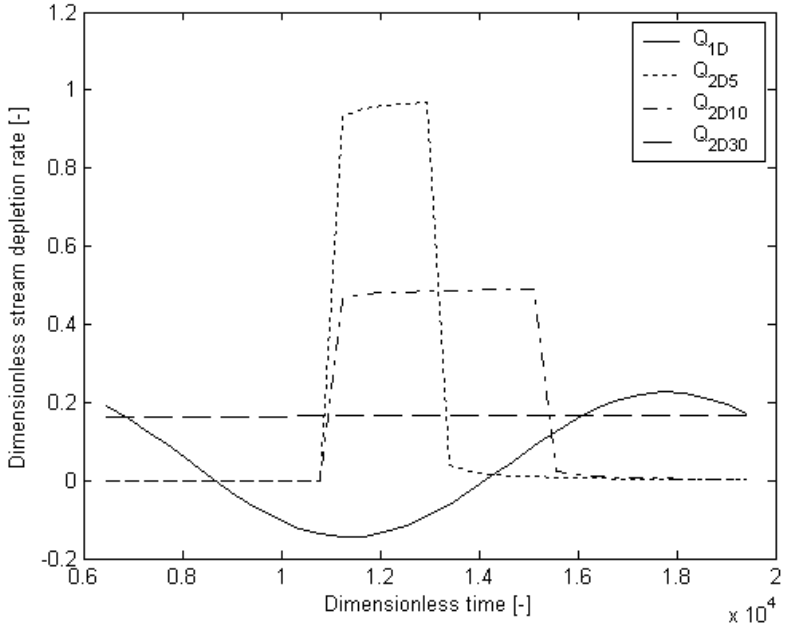

Figure 2.7 Q_{1D} and Q_{2Dj} where subscript j refers to number of days of pumping with Q_0 of 1,000m^3/d and ω of $2\pi/30$ d^{-1}.

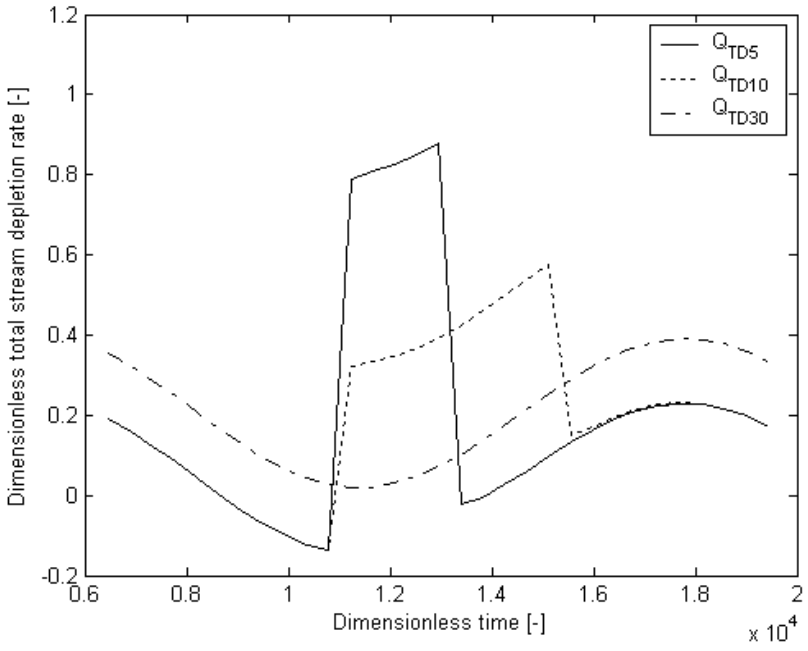

Figure 2.8 Q_{TDj}, with Q_0 of 1,000m^3/d and ω of $2\pi/30$ d^{-1}.

2.5.2 Seasonal stream depletion with streambed

Applying Laplace transform Eq. (2.40) and substituting into Eq.(2.34), the total stream depletion of a case with a streambed is

$$\overline{Q}_{TD} = \frac{CY_D\lambda}{4\pi}\left(\frac{\omega_D^2}{\sqrt{p}\left(p^2+\omega_D^2\right)}\right)\frac{\sqrt{\mu}\cosh\left(\sqrt{\mu p}B'_D\right)+\lambda\mu\sinh\left(\sqrt{\mu p}B'_D\right)}{\sinh\left(\sqrt{\mu p}B'_D\right)+\lambda\sqrt{\mu}\cosh\left(\sqrt{\mu p}B'_D\right)} + \frac{\lambda\overline{Q}_D\sqrt{\mu}e^{-\sqrt{p}x_{WD}}}{\sinh\left(\sqrt{\mu p}B'_D\right)+\lambda\sqrt{\mu}\cosh\left(\sqrt{\mu p}B'_D\right)} \quad . \tag{2.42}$$

Similar to the case without streambed, the stream depletion caused by stream stage fluctuation is numerically calculated using the de Hoog method for inverse Laplace transform. Hantush's (1965) solution for stream depletion caused by a pumping well

with a constant pumping rate is $q/Q_0 = erfc\left(\frac{1}{2\tau}\right) - \exp\left(\frac{1}{2}\eta + \frac{1}{4}\eta^2\tau^2\right) erfc\left(\frac{1}{2\tau} + \frac{1}{2}\eta\tau\right)$

where $\tau = (1/x_w)\sqrt{tK_x/S_s}$ and $\eta = \frac{x_w K'}{2K_x B'}$.

Using the same pumping schemes and the same stream stage fluctuation function as in the cases without the streambed (Figure 2.3, page 32), the dimensionless stream stage and the dimensionless pumping rate are the same as shown in Figure 2.3 as well. Streambeds are 0.2m thick with a hydraulic conductivity of 0.008 m/d and a specific storage of 0.0005 m^{-1}, and the rest of parameters have the same values as for the case without the streambed (Table 2.2, page 32). Pumping rate, frequency of the flood, and stream length that were used to evaluate Q_{1D} would affect results as in the case without the streambed. The shapes of Q_{1D} and Q_{TDj} should be similar to those for the case without the streambed, but have smaller amplitudes. For Q_0 = 1,000m^3/d, $Q_{1D\max}$ is 0.071, $Q_{TD2\max}$ is 0.965, $Q_{TD4\max}$ is 0.519, and $Q_{TD12\max}$ is 0.236. Percentages of $Q_{1D\max}$ to $Q_{TDj\max}$ for pumping periods of 2, 4 and 12 months are 7.3, 13.6, and 30% respectively. $Q_{1D\max}$ and percentages of $Q_{1D\max}$ to $Q_{TDj\max}$ with streambeds are approximately 3% smaller than the ones without the streambed, given the same pumping rate. Changing the streambed thickness to 1 m, $Q_{1D\max}$ and percentages of $Q_{1D\max}$ to $Q_{TDj\max}$ with the streambed are both approximately 16% smaller than the ones without the streambed. The influence of streambed on stream depletion depends on its thickness and hydraulic properties.

2.5.3 Short-term stream depletion without streambed

To study stream-aquifer interaction for a short-term floodwave, one first has to find adequate functions describing stream stages. The following function is a proposed example of a stream stage function:

$$h_S(y,t) = \frac{A_0}{2\sqrt{\pi D t}} e^{-\frac{(y-vt)^2}{4Dt}} . \qquad (2.43)$$

where A_0 is a factor related to amplitude of the floodwave [L^2], D is a factor related to the diffusion of the floodwave [L^2/T], v is a factor relate to velocity of the floodwave along the stream channel[L/T]. This function is used to represent stream stage because of its simplicity and its similar characteristic to hydrograph. Chanson (2004, Eq. 8.11) has investigated the diffusion equation for the open channel flow, and has used a similar form as Eq. (2.43). This equation is identical to the one used to describe the diffusion of a pulse source contaminant transport in groundwater. Figure 2.9 shows an example of the dimensionless stream stage, h_{SD}, as a function of y_D at 1, 5, 10 , and 24 hrs after the floodwave arrived with the following values of parameters: A_0 of $1.5 \times 10^5 m^2$, D of $4 \times 10^5 m^2/d$, v of 8×10^2 m/d. The other parameters are listed in Table 2.2 (page 32). These values are chosen so that the stream stage is approximately 2 m at y_D of 0 after 1 hr. These values are not unique. Other sets of values can produce the same result. Figure2.10 shows h_{SD} as a function of dimensionless time at various distances along a stream (0, 500 m, and 1,000 m) with the same parameters as those used in Figure 2.9. One can replace this stream stage function by any desired functions. If a different stream stage function, which cannot be solved analytically is used, one can always

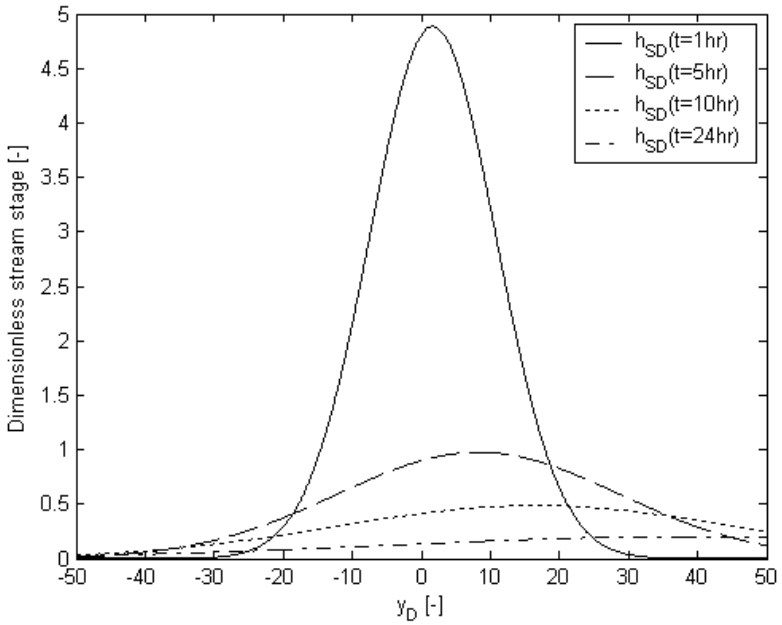

Figure 2.9 Dimensionless stream stages, h_{SD}, as a function of dimensionless distance along the stream at various times.

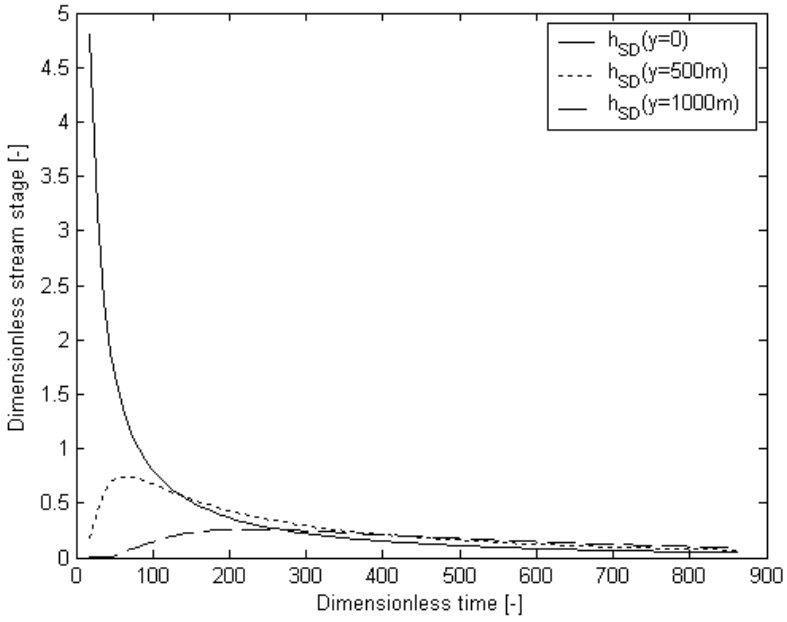

Figure 2.10 h_{SD} as a function of dimensionless time at various distances along the stream.

divide the entire duration of time into many small time intervals and numerically solve the Laplace and inverse Laplace transforms by modifying the Matlab code of the seasonal case. The code solves the stream depletion caused by stream stage fluctuations numerically using the de Hoog inverse Laplace transform method (de Hoog et al., 1982, Hollenbeck, 1998). A constant rate of Q_0 equaling 1,000m^3/d is used to simulate an irrigation or a municipal well, as in section 2.5.1.

More realistic floodwave functions are based on unsteady open-channel flow models, which are often complex and require numerical methods to handle. If a stream has a lateral extension that is much smaller than the longitudinal extension, a one-dimensional unsteady open-channel flow equation can be used, and the most common model is proposed by Saint-Venant (Chow, 1959, Akan, 2006). The difficulty of this approach is that additional parameters need to be specified. If the Froude number, a ratio of square root of the inertial force over the weight of the fluid, is sufficiently low, then the diffusion flood model can be used. The primary advantage of the diffusion model is that effect of the cross-sectional shape of the channel has secondary effect on the floodwave pattern (Rutschmann and Harger, 1996). Rutschmann and Hager (1996) have also discussed in detail about various floodwaves for different stream cross-sectional shapes.

Converting the head in the stream to drawdown, one obtains

$$H_{SD} = H_S \frac{4\pi B\sqrt{K_x K_y}}{Q_0} = \frac{-2\sqrt{\pi K_y}A_0 K_x}{Q_0\sqrt{DS_s}} \frac{1}{\sqrt{t_D}} e^{-\frac{\frac{K_x^2}{4DS_s K_y}(y_D - v_D t_D)^2}{t_D}}, \quad (2.44)$$

where $v_D = \frac{BS_s}{K_x}\sqrt{\frac{K_y}{K_x}}v$. Eq. (2.43) is rewritten as

$$H_{SD} = -C_1 \frac{1}{\sqrt{t_D}} e^{-\frac{C_2(y_D - v_D t_D)^2}{t_D}}, \tag{2.45}$$

where $C_1 = \frac{2\sqrt{\pi K_y} A_0 K_x}{Q_0\sqrt{DS_s}}$, and $C_2 = \frac{K_x^2}{4DS_s K_y}$. Rearranging Eq. (2.45) leads to

$$H_{SD} = -C_1 e^{2C_2 v_D y_D} e^{-C_2 v_D^2 t_D} \frac{1}{\sqrt{t_D}} e^{\frac{-C_2 y_D^2}{t_D}}.$$

Conducting the Laplace transform of H_{SD} by using the following property:

$f(p-a) = L\left(e^{at}F(t)\right)$, where $a = -C_2 v_D^2$ and $F = \frac{1}{\sqrt{t_D}} e^{\frac{-C_2 y_D^2}{t_D}}$, one has

$$\overline{H}_{SD} = -C_1\sqrt{\frac{\pi}{p + C_2 v_D^2}} e^{-2\sqrt{C_2 y_D^2 (p + C_2 v_D^2)} + 2C_2 C_3 y_D} = -C_1\sqrt{\frac{\pi}{p + C_2 v_D^2}} e^{-2\sqrt{C_2 p}|y_D|}. \tag{2.46}$$

Carrying out the Fourier transform of Eq. (2.45), $F\left(e^{-a|y|}\right) = \frac{1}{\pi}\frac{a}{f_y^2 + a^2}$ which is a Lorentzian function, the result is

$$\overline{\overline{H}}_{SD} = -\frac{C_1}{\sqrt{\pi}}\sqrt{\frac{1}{p + C_2 v_D^2}}\frac{2\sqrt{C_2 p}}{f_y^2 + 4C_2 p}. \tag{2.47}$$

Substituting Eq. (2.47) into Eq. (2.16) and setting $f_y = 0$, one got

$$\overline{Q}_{TD} = \frac{C_1}{4\sqrt{\pi C_2}}\sqrt{\frac{1}{p + C_2 v_D^2}} + Q_0 e^{-x_{wD}\sqrt{p}}. \tag{2.48}$$

Conducting the inverse Laplace transform of Eq. (2.48) leads to the following analytical solution:

$$Q_{TD} = \frac{C_1}{4\pi\sqrt{C_2 t_D}} e^{-C_2 v_D^2 t_D} + erfc\left(\frac{1}{2\tau}\right) = \frac{A_0 K_y}{Q_0\sqrt{\pi t_D}} e^{-\frac{S_s B^2 v^2}{4DK_x} t_D} + erfc\left(\frac{1}{2\tau}\right), \quad (2.49)$$

where $\tau = (1/x_w)\sqrt{tK_x / S_s}$.

Figure 2.11 shows Q_{1D} and Q_{2D} after 10 hrs using the same parameters as in Figure 2.9. Because the stream stage at *y* of zero increases rapidly toward infinity as time approaches zero (Figure 2.10, page 43), early stream depletion rates have unrealistically large values. Hence, Figure 2.11 only shows late time results after 10 hrs or t_D of 180. At t_D of 180, Q_{1D} is 0.033 and Q_{2D} is 0.895for Q_0 of 1,000m^3/d. Q_{1D} accounts for 3.6% of the total stream depletion.

As a minor point, we have noticed that changing one or more parameters of the floodwave function can greatly alter the shape of the floodwave. We have tried different possible floodwave functions and found out that using fractional forms, such as $h_S = \frac{A_0}{2(\pi Dt)^{0.2}} e^{-\frac{(y-vt)^{1.3}}{4Dt}}$, one could achieve more realistic shapes of floodwave. Such fractional forms of the floodwave are the empirical formulae which still need to be explained from an open-channel flow model. Functions with fractional terms are generally more difficult to solve.

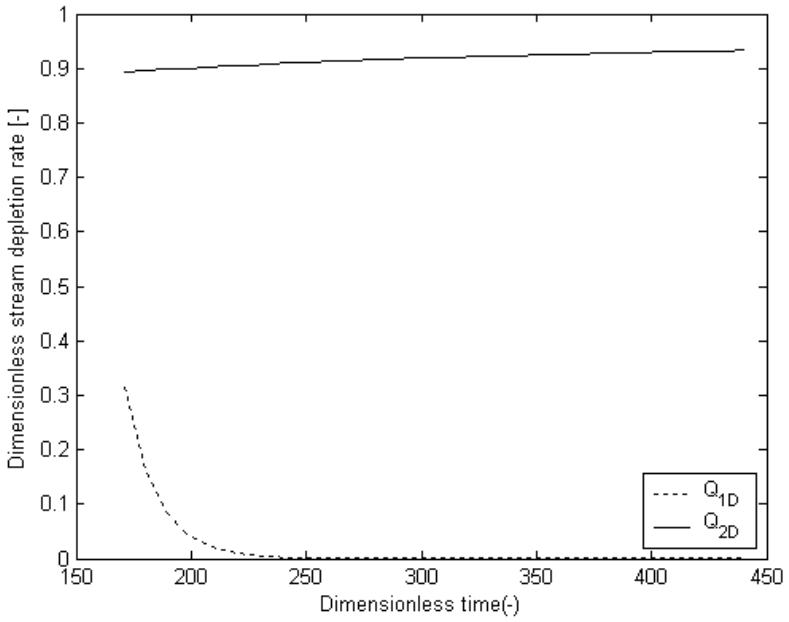

Figure 2.11 Q_{1D} and Q_{2D} with Q_0 of 1,000m^3/d for an individual floodwave.

2.5.4 Short-term stream depletion with streambed

Substituting Eq. (2.47) into Eq. (2.17) and setting $f_y = 0$, one has

$$\overline{Q}_D = \frac{C_1}{8\pi\sqrt{\pi C_2}} \frac{1}{\sqrt{p^2 + C_2 v_D^2 p}} \left(\frac{-\lambda\mu\sqrt{p}\sinh\left(\sqrt{\mu p}B'_D\right) + \sqrt{\mu p}\cosh\left(\sqrt{\mu p}B'_D\right)}{\sinh\left(\sqrt{\mu p}B'_D\right) + \lambda\sqrt{\mu}\cosh\left(\sqrt{\mu p}B'_D\right)} \right) + \frac{\lambda\overline{Q}_0\sqrt{\mu p}e^{-\sqrt{p}x_{WD}}}{\sqrt{p}\sinh\left(\sqrt{\mu p}B'_D\right) + \lambda\sqrt{\mu p}\cosh\left(\sqrt{\mu p}B'_D\right)} \quad (2.50)$$

Q_{1D} is numerically solved using the de Hoog inverse Laplace transform method. Q_{2D} is the same as the Hantush's (1965) analytical solution which

is $Q_{2D} = erfc\left(\frac{1}{2\tau}\right) - \exp\left(\frac{1}{2}\eta + \frac{1}{4}\eta^2\tau^2\right) erfc\left(\frac{1}{2\tau} + \frac{1}{2}\eta\tau\right)$, where $\tau = (1/x_w)\sqrt{t\ K_x / S_s}$, and $\eta = \frac{x_w K'}{2K_x B'}$.

The thickness of the streambed is 0.2 m with its conductivity of 8.64×10^{-3}m/d and storage of 0.01. The shape of Q_{1D} and Q_{2D} with the streambed is the same as in the case without the streambed. At t_D of 180, Q_{1D} is 0.029 and Q_{2D} is 0.895 using the same hydraulic parameters as in the case without the streambed. The actual value of Q_{1D} is 12% lower than that in the case without the streambed. Q_{1D} accounts for 3.2% of the total stream depletion comparing to 3.6% of the case without the streambed. The values of Q_{2D} are the same as those without the streambed because the streambed only has significant effects at the early time and its influence to stream depletion gradually disappear when pumping sufficiently long time.

2.5.6 Early and late time approximations of Q_{1D}

The early time approximation of Q_{1D} can be calculated by letting p in Eq. (11) approaches ∞, and the late time approximation of Q_{1D} can be calculated by letting p in Eq. (11) approaches zero. The early time approximation is used when the pumping well is initially turned on and the late time approximation is used after the pumping well was on for a long period of time. To obtain results, one must specify the stream stage function. Using the stream stage function described in Eq. (2.39), when $p \to \infty$, Eq. (2.41) becomes (neglecting the second term on the right hand by shutting down the pumping well):

$$\overline{Q}_{1D} = \frac{CY_D \omega_D^2}{4\pi} p^{-\frac{5}{2}}. \tag{2.51}$$

The inverse Laplace transform of Eq. (2.50) will lead to the analytical solution in the real time domain as

$$Q_{1D} = \frac{CY_D \omega_D^2}{3\pi\sqrt{\pi}} t_D^{3/2}. \tag{2.52}$$

When $p \to 0$, Eq. (2.41) becomes (setting the pumping rate to zero)

$$\overline{Q}_{1D} = \frac{CY_D}{4\pi} p^{-\frac{1}{2}}. \tag{2.53}$$

The inverse Laplace transform of Eq. (2.52) will lead to the analytical in the real time domain as

$$Q_{1D} = \frac{CY_D}{4\pi\sqrt{\pi t_D}}. \tag{2.54}$$

Eq. (2.54) shows that the late time approximation of Q_{1D} is decaying with time in a fashion that is inversely proportional to the square root of time. This leads to an important conclusion that Q_{1D} can be neglected for a stream aquifer system that has years to equilibrate.

2.6. Summary and Conclusions

Chapter II considers drawdown and stream depletion caused by a fully penetrating pumping well near a fully penetrating stream with and without the streambed. General solutions of drawdown in the aquifer in the Laplace-Fourier domain with and without streambeds for any pumping schedules and any stream stage functions

were presented. We consider two general stream stage functions. For the seasonal fluctuation case, the stream stage is a function of time only. For the short-term fluctuation case, the stream stage depends on time and distance along the stream. The following function: $h_S(t) = A\left(1-\cos(\omega t)\right)$ is used to describe the seasonal stream stage variation. We present semi-analytical stream depletion rates (in time domain) using a numerical method to solve for stream depletion caused by stream stage fluctuations and using an analytical method to solve for stream depletion caused by a pumping well for both with and without streambed sediments.

Three primary factors affecting the stream depletion caused by stream fluctuations are the pumping rate, the frequency of the flood, and the stream length that is used to evaluate the stream depletion. The period of stream fluctuation plays a crucial role in affecting the stream depletion. A shorter period yields a grater rate of stream depletion caused by stream stage fluctuation.

If a streambed exists, it can greatly reduce stream depletion caused by stream stage fluctuations; however, if pumping time is long enough, the stream depletion rate caused by the extraction well is insensitive to the streambed parameters.

For the short-term floodwave fluctuation, general solutions of drawdown in the aquifer in the Laplace-Fourier domain with and without streambed for any pumping schedules and any stream stage functions are presented. The following function: $h_S(y,t) = \frac{A_0}{2\sqrt{\pi Dt}} e^{-\frac{(y-vt)^2}{4Dt}}$ is used to describe the short-term stream stage fluctuations. An analytical stream stage depletion rate in real time domain is presented for the case

without the streambed. The stream depletion rate for the case with the streambed is solved in the same manner as the seasonal fluctuation case.

We have derived the analytical solutions of the stream depletion rates at early and late times caused by stream fluctuation following a cosine function. It is interesting to point out that the late time stream depletion decays with time as a fashion that is inversely proportional to the square root of time. This implies that the stream depletion caused by stream stage fluctuation can be neglected for a stream aquifer system that has years to equilibrate. At late times, the pumping well becomes the dominating factor for influencing the stream depletion. At early time, however, the contributions from both the stream stage fluctuation and the pumping well have to be considered.

This dissertation showed that the drawdown and stream depletion rate can be written in two separated terms and can be solved independently. If one would like to add additional component, it can be done by superposition another term in the existing result.

CHAPTER III

CAPTURE ZONE BETWEEN TWO STREAMS*

We have investigated stream-aquifer interaction with a single pumping well in an aquifer bounded by two parallel nearby streams. This study presents steady-state semi-analytical solutions to calculate the fraction of water withdrawal from two streams. Potential theory is used to describe the capture zone between two streams when low-permeability streambeds are not present. Steady-state flow equations in the aquifer and two streambeds are solved following rigorous mass balance requirements if low-permeability streambeds are present. When the low-permeability streambeds are not present and the regional flow exists between two streams, this study finds that the maximal capture size without extracting water from the down-gradient stream decreases with the normalized well location in an approximately linear fashion. Furthermore, the normalized flux from the up-gradient stream decreases with the normalized well location faster than the linear fashion. When the low-permeability streambeds exist and the regional flow is neglected, the normalized flux across either streambed varies with the normalized well location in a linear function. Furthermore, the magnitude of the slope of that function is nearly unity when the hydraulic conductance ratio of the two streambeds is one and is less than unity when the hydraulic conductance ratio of the two streambeds is either greater or smaller than one. When the normalized well location with equal

---

* Reprinted with permission from "Capture Zone between two Streams" by Trin Intaraprasong and Hongbin Zhan, 2007, Journal of Hydrology, 338, p. 297-307,

fluxes from two streams versus the hydraulic conductance ratio of the two streambeds are plotted semi-logarithmically, we observed a segmented curve including a steep segment at the beginning, followed by a flat segment, and a final steep segment.

3.1 Introduction

A capture zone refers to an aquifer volume in which water can be extracted by one or multiple pumping wells penetrating the aquifer under steady-state flow condition. Studies of capture zones have continued for several decades because of their practical importance. For example, wellhead protection plans must rely on good understanding of the capture zones of the pumping wells. Groundwater remediation designs using the pump-and-treat method often need information about the capture zones of the extraction wells.

The study of capture zones can be dated back to the original work of Muskat (1946) with the use of the potential theory. Since then, many scientists have made important contributions in this field (Polubarinova-Kochina, 1962; Bear, 1972; 1979). A significant amount of work has been carried out using analytical approaches to describe capture zones of vertical pumping wells without considering the lateral boundaries of the aquifer (Javandel and Tsang, 1986; Shafer, 1987; Lerner, 1992; Grubb, 1993; Faybishenko et al., 1995; Schafer, 1996; Shan, 1999; Zhan, 1999a; Christ and Goltz, 2002; Cunningham et al., 2004; Luo and Kitanidis, 2004). Numerical simulations can take into account complex boundary conditions as well as heterogeneity, recharge/discharge, etc., thus are also broadly used for studying vertical well capture zones (Ahlfeld and Sawyer, 1990; Bair and Roadcap, 1992; Tiedeman and Gorelick,

1993). In recent years, there are several studies related to the capture zone of a horizontal well (Schafer, 1996; Steward, 1999; Zhan, 1999b; Zhan and Cao, 2000; Kompani-Zare et al., 2005). Scientists have used stochastic methods to study capture zones in heterogeneous aquifers (Zhang and Lu, 2004).

The capture zone of single or multiple groundwater extraction wells near a stream is also of interest to hydrologists. The capture zone of a pumping well near a stream might be obtained in a straightforward manner by using an image well under rather strict constrains such as perfect connection between the stream and the aquifer and full stream penetration (Newsom and Wilson, 1988).

The strong interest of studying capture zone near a stream comes from several needs. For instance, the pumping induced stream depletion can significantly alter the water budget of the surface water, thus is important in terms of water resources management (Granato and Barlow, 2004). Groundwater extraction from an aquifer near a stream can also impact the ecologic environments of the riparian zones and the river-bank wetlands, thus is of great concern to the ecologists as well as many others (Winter et al., 1998; Wurster et al., 2003).

Under certain field conditions, a pumping well may be located between two parallel streams. This situation can occur when two channels or two tributaries are closely spaced. It can also occur in some engineered structures such as two parallel water canals. As shown in Chen and Chen (2003a, 2003b), in certain areas of the High Plains of the United States, two streams can be parallel and the distance between them could be as close as 270m. If a pumping well is located between two parallel streams, the shape of

the capture zone will depend on stream depletions from both streams, which is an important issue in water rights adjudication. Kollet (2005) has pointed out that inadequate application of a single stream model to deal with a two-stream system might lead to an error of stream depletion.

Wilson (1993) has studied induced infiltration in aquifers with ambient flow. In that study, he has also discussed well pumping from an aquifer bounded by a stream and a barrier, and well pumping from an aquifer bounded by two parallel streams. The vertical recharge is considered, but the semi-pervious streambeds are not considered in that study. Wilson (1993) has adopted the Schwartz-Christoffel Conformal mapping method to deal with the two streams which are regarded as constant-head boundaries. Zlotnik (2004) has also dealt with well pumping between two streams and has proposed the concept of maximum stream depletion rate (MSDR) to account for the leakage from the underlying aquitard.

To our knowledge, there are still no studies that concern capture zone between two parallel streams considering the low-permeability streambeds. The purpose of this study is to analytically study capture zone between two parallel streams. Two different kinds of stream-aquifer interfaces will be considered: one has perfect hydraulic connection between the stream and the aquifer, and the other has low-permeable sediments clogging the streambeds. The perfectly connected stream-aquifer scenario might be found in Northwest States of the United States such as Montana where streambeds are often composed of coarse sediments (Woessner, 2000). The clogged streambed scenario frequently appears in the alluvial or glacial aquifers (Larkin and

Sharp, 1992; Conrad and Beljin, 1996). We are interested to see how the two streams control the shape of the capture zone, and how the low permeable streambeds might affect stream depletion from both streams. This study is limited to the steady-state flow condition whereas the transient flow problem will be addressed by Sun and Zhan (2007).

3.2 Model Descriptions

A realistic capture zone between two streams could be very complicated because of many issues such as meandering of stream channels, variation of water level in the streams, heterogeneity of streambeds and aquifer, partially penetrating streams, etc. Such complex setting requires numerical simulations. Analytical models can be used as the first screening tool for the problem and can offer better insights into the problem. To make the analytical models amendable, some assumptions are inevitable. These include: (1) the stream stages are approximately stable; (2) the aquifer has no leakage through upper or lower layers; (3) the well fully penetrates the aquifer and is pumped at a constant rate; (4) the aquifer is homogeneous and horizontally isotropic; and (5) the Dupuit assumption is valid. These assumptions can be relaxed under certain circumstances. For instance, the horizontally isotropic assumption can be relaxed to include the horizontally anisotropic media. Bear (1972, 1979) have provided details on how to deal with an anisotropic aquifer.

Another important issue that must be addressed is the treatment of the stream penetration. Many studies using image wells to deal with streams treat the streams as fully penetrating constant-head boundaries (Theis, 1941; Glover and Balmer, 1954; Jenkins, 1968; Bear, 1972, 1979; Newsom and Wilson, 1988). Hantush (1965) has

included semi-permeable streambeds in studying a fully penetrating stream. In reality, it is better to characterize streams as partially penetrating with finite widths. Hunt (1999) has proposed a model that considered a very shallow stream with an infinitesimal width. Zlotnik et al. (1999) and Butler et al. (2001) have investigated a partially penetrating stream with a finite width. The advantage of the partially penetrating stream models of Hunt (1999), Zlotnik et al. (1999), and Butler et al. (2001) is that these models can provide solutions beyond the streams, whereas the fully penetrating models of Theis (1941), Glover and Balmer (1954), Jenkins (1968), and Hantush (1965) cannot. Indeed, from a three-dimensional view of groundwater movement in a stream-aquifer system, the scenario of flow from a partially penetrating stream is different from that from a fully penetrating stream. However, many present models of stream-aquifer interaction, including Hunt (1999), Zlotnik et al. (1999), and Butler et al. (2001) have adopted the Dupuit assumption, meaning that the vertical flow is neglected. Such an assumption has substantially simplified the problem.

First, the models of partially penetrating streams with finite widths developed by Zlotnik et al. (1999) and Butler et al. (2001) were found to be close to the mathematically simpler model of Hunt (1999) for zero-depth penetrating and zero width streams under many practical circumstances. Second, if one adopts the Dupuit assumption, the Hunt's solution (1999) is identical to that of Hantush (1965) for a fully penetrating stream. This is because one cannot distinguish the geometric difference of a partially penetrating stream from a fully penetrating stream under the Dupuit assumption. The geometric difference can only be addressed in the case of a three-

dimensional flow field (Sun and Zhan, 2007). In fact, several scientists including Hunt himself have noticed the identity of the Hunt's solution (1999) and that of Hantush (1965) after a simple parameter transformation. Such an identity indicates that the fully penetrating stream model, despite its disadvantage of not representing a partially penetration stream, can yield the same solution as the partially penetrating stream model at the region bounded by the streams, provided that the Dupuit assumption is employed. This implies that the study presented here can be used for both fully penetrating and partially penetrating streams as long as the Dupuit assumption is adopted (Sun and Zhan, 2007). Two different cases without and with low-permeability streambeds will be addressed.

Figure 3.1 is a schematic diagram of a vertical pumping well in a confined aquifer with a perfectly connected stream-aquifer system. We denote the left stream and right stream as stream 1 and stream 2, respectively. The *x*- and *y*-axes are perpendicular and parallel to the streams, respectively. The origin of the coordinate is at the stream1 and the *x*-axis passes through the center of the pumping well. The aquifer is of infinite extend along the *y*-axis. The two streams might have different stages. We arbitrarily allow stream1 to have a higher stage (h_1) than that of stream 2 (h_2), thus a regional flow, *q*, from left to right exists. The streams 1 and 2 are therefore named the up-gradient and down-gradient streams, respectively. The pumping well is located at distance "*a*" from the origin and the two streams are apart by a distance *L*.

After activating the pumping well with a pumping rate *Q* for some time, the cone of depression will expand and eventually will reach the stream(s). At the steady-

state, all the pumped water comes from the two streams. Since the well could extract water from both streams, it is necessary to know the percentage of water extracted from each stream. The setting in Figure 3.1 requires an infinite number of image wells to simulate two parallel streams. If low-permeability streambeds exist, it would be difficult to use image wells to study the capture zone. Instead, we will proceed by directly solving the boundary value problem considering two semi-pervious streambeds of finite thickness at the stream-aquifer interfaces.

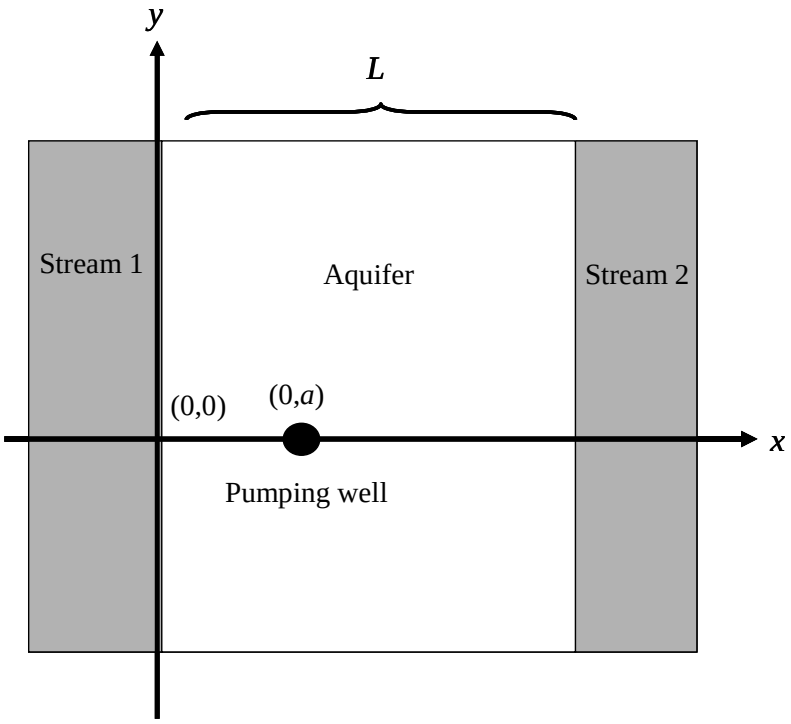

Figure 3.1 Schematic diagram of pumping between two streams without low-permeability streambeds. A uniform regional flow is from left to right. Streams 1 and 2 are named up-gradient and down-gradient streams.

3.3 Mathematical Formulation without Low-permeability Streambed Sediment

3.3.1 Potentials and streamlines of the capture zone

An envelope of capture zone is defined as the boundary that separates the regions flowing to and bypassing the well and it defines the shape and the size of the capture zone (e.g. Shan, 1999; Kompani-Zare et al., 2005). As done in many previous studies, we devise an appropriate complex potential, $\zeta(z)$, for the flow field to find the capture zone (Bear, 1972, 1979). $\zeta(z) = \phi + i\psi$, and ϕ and ψ are the real and imaginary parts describing potential and stream functions respectively, and $i = \sqrt{-1}$ is the sign of complex. The potential is associated with the hydraulic head, *h*, as $\phi = Kh$, where *K* is the hydraulic conductivity. The stream function defines the flow pathways. We first need to find the stagnation point which has a zero flow velocity. The stagnation point can be found by letting the first derivative of the complex potential with respect to the complex variable, *z*, to be zero (e.g. Shan, 1999; Kompani-Zare et al., 2005). The streamlines passing through the stagnation point describe the envelope of the capture zone. Furthermore, the amount of water flow into the well is equal to the difference of the values of the two streamlines describing the envelope of the capture zone (Bear, 1972).

Assuming steady-state uniform regional flow in a homogeneous, isotropic, and laterally infinite confined aquifer of uniform thickness, we can use complex potential theory to describe flow to a pumping well with a constant rate located at the origin of the coordinate system as (Bear, 1972):

$$\zeta(z) = m\ln(z) - qz, \tag{3.1}$$

where $z = x + iy$ is the complex argument, $m = Q/2\pi B$, Q is the pumping or injection rate (positive for pumping and negative for injecting), and B is the aquifer thickness. We are going to define the following normalized (dimensionless) terms and from now on to precede the calculation in normalized forms.

$$x_D = \frac{x}{L}, y_D = \frac{y}{L}, z_D = \frac{z}{L}, \; a_D = \frac{a}{L}, Q_D = \frac{Q}{2\pi BLq}, \zeta_D = \frac{\zeta}{qL}, \phi_D = \frac{\phi}{qL}, \psi_D = \frac{\psi}{qL}, \qquad (3.2)$$

where the subscript "D" denotes the normalized term in Eq. (3.2).

Eqs. (3.1) and (3.2) can be reformulated for an unconfined aquifer when flow is primarily horizontal. For that case, the saturated thickness varies and a new potential $\phi = Kh^2/2$ is defined, where K is the hydraulic conductivity and h is the hydraulic head (Bear, 1972, 1979; Wilson, 1993). For the unconfined aquifer, the product of Bq has to be replaced by the discharge per unit width, q_a [L^2/T] (Wilson, 1993). The dimensionless Q_D, ζ_D, ϕ_D, and ψ_D have to be redefined as $Q_D = Q/(2\pi L q_a)$, $\zeta_D = \zeta / q_a$, $\phi_D = \phi / q_a$, and $\psi_D = \psi / q_a$. The above Eq. (3.1) is replaced by $\zeta(z) = (Q/2\pi)\ln(z) - q_a z$. As pointed out by Wilson (1993), the solution, in particularly the stream depletion is indifferent to the definition of ϕ and to whether the aquifer is assumed to have a constant transmissivity or one that varies with saturated thickness. Therefore, we will only focus on the discussion of a confined aquifer for the rest of the paper.

On the basis of Eqs. (3.1) and (3.2), we can use an infinite number of image wells to simulate the parallel streams which are assumed as constant head boundaries (Bear, 1972). The image well configuration is shown in Figure 3.2 and the result is

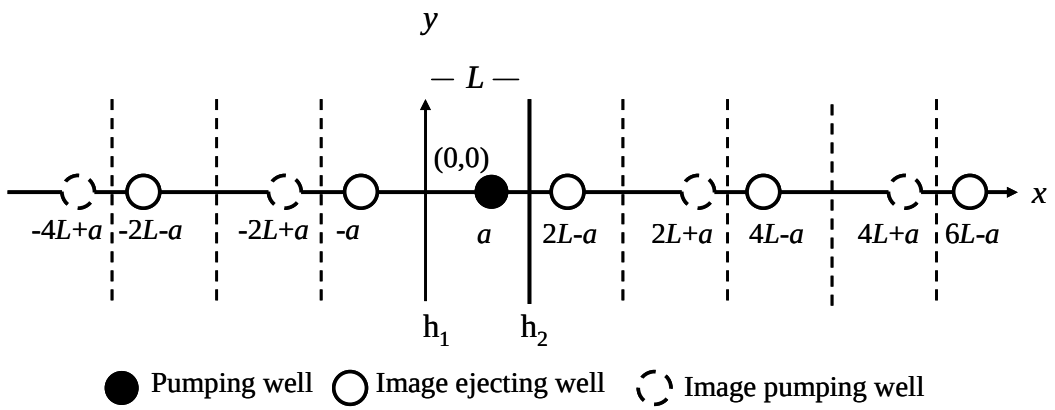

Figure 3.2 Schematic diagram showing a real pumping well and an infinite series of image pumping and injecting wells to represent the two stream boundaries

$$\zeta_D(z) = Q_D \sum_{n=-\infty}^{\infty} \left[\ln[z_D - (a_D + 2n)] - \ln[z_D - (-a_D + 2n)] \right] - z_D , \tag{3.3}$$

where n are integers. Using the same method as Zhan (1999b) to calculate the summation term in Eq. (3.3), one obtains

$$\zeta_D(z) = Q_D \ln\left[\frac{\sin\left(\pi(z_D - a_D)/2\right)}{\sin\left(\pi(z_D + a_D)/2\right)} \right] - z_D . \tag{3.4}$$

Separating the real part from the imaginary part, the results are

$$\phi_D = \frac{Q_D}{2} \ln\left[\frac{\cosh\left(\pi y_D\right) + \cos\left(\pi(x_D - a_D)\right)}{\cosh\left(\pi y_D\right) + \cos\left(\pi(x_D + a_D)\right)} \right] - x_D , \tag{3.5}$$

$$\psi_D = Q_D \tan^{-1}\left[\frac{\sin\left(\pi a_D\right)\sinh\left(\pi y_D\right)}{\cos\left(\pi a_D\right)\cosh\left(\pi y_D\right) + \cos\left(\pi x_D\right)} \right] - y_D , \tag{3.6}$$

where ϕ_D is the velocity potential, and ψ_D is the stream function, all in normalized forms. Bruggeman (1999, p.312, solution 356.12) has provided the solutions of pumping

between two streams in slightly different formulations without considering the regional flow. It is easy to prove that Bruggeman's (1999) complex potential function is identical to ours after simple change of notation and neglect of the regional flow. Bruggeman (1999) expressed the drawdown as an infinite series of terms whereas we use above Eq. (3.5) for the potential.

3.3.2 Stagnation point and critical pumping rate

To find the stagnation point, we take the first derivative of the complex potential (Eq. (3.4)) with respect to z_D and set it to zero. The result is

$$\cos(\pi z_{0D}) = \cos(\pi a_D) - \pi Q_D \sin(\pi a_D), \tag{3.7}$$

where z_{0D} is the complex variable at the stagnation point. Eq. (3.7) reflects some interesting features of the stagnation point and the capture zone between two streams. The absolute value of $\cos(\pi z_{0D})$ in Eq. (3.7) could be less than, or greater than, or equal to unity, corresponding to three possible cases that will be discussed as follows.

For the first case, the condition $-1 < \cos(\pi z_{0D}) < 1$ is satisfied and the complex variable z_{0D} reduces to a real variable, x_{0D}, indicating that the stagnation point is located at the *x*-axis between two streams. Notice that $Q_D > 0$ for a pumping well and $0 < a_D < 1$, thus $\pi Q_D \sin(\pi a_D) > 0$, which leads to $\cos(\pi x_{0D}) < \cos(\pi a_D) < 1$ from Eq. (3.7). Therefore, the condition $\cos(\pi x_{0D}) < 1$ is always satisfied. Furthermore, if recalling the properties of the cosine function, the inequality $\cos(\pi x_{0D}) < \cos(\pi a_D)$ indicates that $x_{0D} > a_D$. This implies that there is a single stagnation point located at the *x*-axis somewhere between the pumping well and stream 2, and the extracted water comes entirely from stream 1.

The coordinate of that stagnation point is

$$z_{0D} = x_{0D} = \frac{1}{\pi}\cos^{-1}\left[\cos(\pi a_D) - \pi Q_D \sin(\pi a_D)\right]. \quad (3.8)$$

To satisfy the condition of $\cos(\pi x_{0D}) > -1$ in Eq. (3.7) for the first case, one has

$$Q_D < Q_{cD} = \frac{1}{\pi}\frac{1+\cos(\pi a_D)}{\sin(\pi a_D)} = \frac{1}{\pi}\cot(\pi a_D / 2), \quad (3.9)$$

where $Q_{cD} = \cot(\pi a_D / 2)/\pi$ is the dimensionless critical pumping rate.

It is interesting to point out that Wilson (1993) has also reported the calculation of the critical pumping rate. It is easy to prove that our solution of Eq. (3.9) is identical to Wilson's solution when one recognizes different definitions of symbols. In Wilson's work (1993, eq. (20b)), the stream on the right is the up-gradient stream, thus regional flow is from right to left. In our study, the up-gradient stream is on the left, thus regional flow is from left to right. Therefore our "a" is the "L-d" in Wilson's work. When recognizing this, the right hand side of Eq. (3.9) is

$\frac{1}{\pi}\cot(\pi a_D / 2) = \frac{1}{\pi}\cot\left(\frac{\pi}{2} - \delta\right) = \frac{1}{\pi}\tan(\delta)$, where $\delta = \pi d / 2L$ is used by Wilson (1993). Our dimensionless pumping rate $Q_{cD} = Q_c /(2\pi BLq) = (1/\pi)\alpha_c$, where Q_c is the critical pumping rate, and α_c is a parameter used by Wilson (1993, eq. (20b)). Therefore, our Eq. (3.9) becomes $\alpha_c = \tan(\delta)$, identical to Eq. (20b) of Wilson (1993).

For the second case, $|\cos(\pi z_{0D})| = 1$, thus $z_{0D} = 1$, which indicates that the stagnation point is located exactly at (x_D =1, y_D =0), and the pumping rate is at the

critical rate $Q_D = Q_{cD}$. This condition corresponds to the maximal possible pumping rate without extracting water from stream 2.

For the third case, $\left|\cos(\pi z_{0D})\right| > 1$. This case is associated with a normalized pumping rate that is greater than $\cot(\pi a_D / 2)/\pi$ and the pumping well extracts water from both streams. Notice that the right hand side of Eq. (3.7) is a real value, thus $z_{0D} = 1 \pm i y_{0D}$, where y_{0D} is a real variable. This indicates that the stagnation points are now at the line of x_D=1. The coordinates of the two stagnation points are:

$$z_{0D} = 1 \pm \frac{i}{\pi} \cosh^{-1}\left[\cos(\pi a_D) - \pi Q_D \sin(\pi a_D)\right]. \tag{3.10}$$

It is also easy to prove that our solution Eq. (3.10) is identical to Eq. (21) of Wilson (1993) for the stagnation points. Substituting the coordinates of the stagnation point into Eq. (3.6), one can find the values of the streamlines passing through the stagnation point. Note that the streamlines connecting at a stagnation point can have different values (Bear, 1972).

3.4 Mathematical Formulation with Low-permeability Streambed Sediment

3.4.1 Problem description

To obtain the drawdown in the aquifer with low-permeability streambeds separating the streams from the aquifer, continuity of head and flux at the aquifer-streambed boundary is used. The streambeds separating the first and the second streams from the aquifer are named streambed 1 and streambed 2, respectively. Figure 3.3 shows

the schematic diagram of this case. Notice that the *y*-axis now is at the interface of the aquifer with streambed 1, and "*L*" now represents the distance between two streambeds.

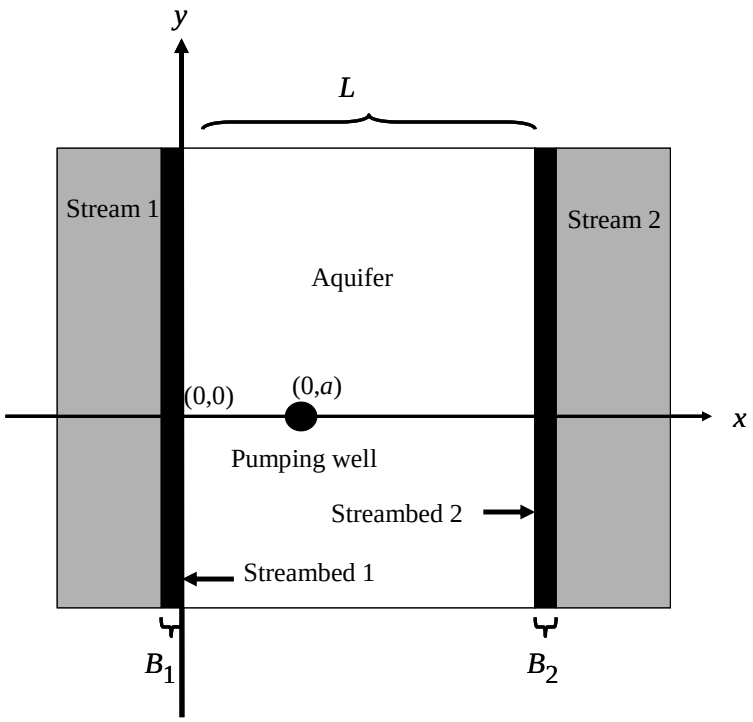

Figure 3.3 Schematic diagram of pumping between two streams with low-permeability streambeds.

B_1 and B_2 in Figure 3.3 are the thickness of the streambeds 1 and 2, respectively. The values of the hydraulic conductivity of both streambeds are assumed to be at least two orders of magnitude smaller than that of the aquifer, thus flows in the streambeds are perpendicular to the aquifer-streambed boundaries. The governing equation and the boundary conditions of steady-state flow to a pumping well in the aquifer are as follows (in normalized forms):

$$\frac{\partial^2 s_D}{\partial x_D^2} + \frac{\partial^2 s_D}{\partial y_D^2} = -4\pi\delta(x_D - a_D)\delta(y_D), \tag{3.11}$$

$$s_D(x_D, y_D = \pm\infty) = 0, \tag{3.12}$$

$$\left.\frac{\partial s_{1D}}{\partial x_D}\right|_{x_D=0} = \beta_1 \left.\frac{\partial s_D}{\partial x_D}\right|_{x_D=0}, \tag{3.13}$$

$$\left.\frac{\partial s_{2D}}{\partial x_D}\right|_{x_D=1} = \beta_2 \left.\frac{\partial s_D}{\partial x_D}\right|_{x_D=1}, \tag{3.14}$$

$$s_{1D}\big|_{x_D=0} = s_D\big|_{x_D=0}, \tag{3.15}$$

$$s_{2D}\big|_{x_D=1} = s_D\big|_{x_D=1}, \tag{3.16}$$

where the associated normalized terms are define as:

$$s_D = \frac{4\pi KBs}{Q}, s_{1D} = \frac{4\pi KBs_1}{Q}, s_{2D} = \frac{4\pi KBs_2}{Q}, B_{1D} = \frac{B_1}{L}, B_{2D} = \frac{B_2}{L}, \beta_1 = \frac{K}{K_1}, \beta_2 = \frac{K}{K_2}, \tag{3.17}$$

where s, s_1, and s_2 are the drawdowns of the aquifer, the streambeds 1 and 2, respectively; K_1 and K_2 are the hydraulic conductivities of the streambeds 1 and 2, respectively; $\delta(\ )$ is the Dirac delta function; and β_1 and β_2 refer to the hydraulic conductivity ratios of the aquifer over the streambeds 1 and 2, respectively. Eq. (3.12) implies that the drawdowns at the points far from the pumping well are zero. Eqs. (3.13) and (3.14) describe the continuity of flow at the aquifer-streambed interfaces and Eqs. (3.15) and (3.16) refer to the continuity of drawdown at the aquifer-streambed interfaces. The streams are at constant stage, thus, $s_{1D}(x_D = -B_{1D}) = 0$ and $s_{2D}(x_D = 1 + B_{2D}) = 0$.

3.4.2 Proposed solutions

Considering the finite width of the aquifer in the *x*-axis, we propose the following solution for s_D based on the finite Fourier transform in the *x* direction.

$$s_D = \sum_{n=0}^{\infty} H_n(y_D)\sin(\omega_n x_D + \mu_n),\ \omega_n > 0, \tag{3.18}$$

where ω_n and μ_n are the spatial frequency and the phase term respectively that will be determined using the boundary conditions, and H_n is a function of y_D. Similar solutions have been used in previous studies of Zhan et al. (2001), Zhan and Zlotnik (2002), and Zlotnik and Zhan (2005) for transient flow problems. If there are no streambeds, μ_n=0; otherwise $\mu_n \neq 0$. To determine H_n, one can first substitute Eq. (3.18) into Eq. (3.11), then multiply Eq. (3.11) by $\sin(\omega_m x_D + \mu_m)$, and integrate both sides of Eq. (3.11) from 0 to 1 for x_D. If applying the following identity

$$\begin{aligned}&\int_0^1 \sin(\omega_n x_D + \mu_n)\sin(\omega_m x_D + \mu_m)dx_D \\ &= \begin{Bmatrix} \frac{1}{2} - \frac{1}{4\omega_n}[\sin(2\omega_n + 2\mu_n) - \sin(2\mu_n)], & n = m \\ 0, & n \neq m \end{Bmatrix},\end{aligned} \tag{3.19}$$

Eq. (3.11) will become

$$\frac{\partial^2 H_n(y_D)}{\partial y_D^2} - \omega_n^2 H_n(y_D) = -\frac{4\pi}{\alpha_n}\sin(\omega_n a_D + \mu_n)\delta(y_D), \tag{3.20}$$

where α_n is

$$\alpha_n = \frac{1}{2} - \frac{1}{4\omega_n}[\sin(2\omega_n + 2\mu_n) - \sin(2\mu_n)]. \tag{3.21}$$

The boundary condition for H_n is obtained by substituting Eq. (3.18) into Eq. (3.12):

$$H_n(y_D = \pm\infty) = 0\,. \tag{3.22}$$

Eq. (3.20) is the modified one-dimensional Helmholtz equation (Arfken and Weber, 1995, p. 516). Considering the boundary condition Eq. (3.22), the solution of Eq. (3.20) is

$$H_n(y_D) = \frac{2\pi}{\alpha_n \omega_n}\sin(\omega_n a_D + \mu_n)\exp(-\omega_n|y_D|). \tag{3.23}$$

Now the remaining question is to find ω_n and μ_n which are solved in Appendix C on page 103. The final solution becomes

$$s_D = \sum_{n=0}^{\infty}\frac{2\pi}{\alpha_n \omega_n}\sin(\omega_n x_D + \mu_n)\sin(\omega_n a_D + \mu_n)\exp(-\omega_n|y_D|). \tag{3.24}$$

The stream depletion can be computed using the drawdown of Eq. (3.24). The stream depletion per unit width along stream 1 can be defined as $q_{s1} = KB\left.\frac{\partial s}{\partial x}\right|_{x=0}$. The total stream depletion from stream 1 is $Q_{s1} = \int_{-\infty}^{+\infty} KB\left.\frac{\partial s}{\partial x}\right|_{x=0} dy$. Using dimensionless terms, one has:

$$\frac{Q_{s1}}{Q} = \frac{1}{4\pi}\int_{-\infty}^{+\infty}\left.\frac{\partial s_D}{\partial x_D}\right|_{x_D=0} dy_D = \sum_{n=0}^{\infty}\frac{1}{\alpha_n \omega_n}\cos(\mu_n)\sin(\omega_n a_D + \mu_n)\,. \tag{3.25}$$

The stream depletion from stream 2 is simply $\frac{Q_{s2}}{Q} = 1 - \frac{Q_{s1}}{Q}$.

4.4.3 Numerical computation

First, we need to determine ω_n and μ_n. To obtain ω_n, we solve Eq. (C13) in Appendix C (page 103) using the Newton-Raphson method (Press et al., 1989). The primary reason for choosing this method is its simplicity and fast convergence. It is necessary to choose an initial guess that are reasonably close to the actual solution because of the oscillation nature of the tangent function in Eq. (C13). For instance, Figure 3.4 plots the left and right hand sides of Eq. (C13) for the case of $\beta_1 = \beta_2 = 0.01,\ B_{1D} = B_{2D} = 0.001$. The intercept points there are the solutions of ω_n. As can be seen from this figure, there is a single solution within each domain $[n\pi - \pi/2, n\pi + \pi/2]$, where *n*=1, 2,… It is crucial to choose close enough initial guesses when $B_{1D}\beta_1 B_{2D}\beta_2\omega_n^2$ is close to unity because $B_{1D}\beta_1 B_{2D}\beta_2\omega_n^2 = 1$ is the singular point of the right hand side of Eq. (C13). After finding ω_n, μ_n can be found from $\mu_n = \tan^{-1}(B_{2D}\beta_2\omega_n)$. Substituting ω_n and μ_n into Eq. (3.24) will lead to the solution.

Our numerical exercises show that using thirty terms in Eq. (3.24) can achieve an accurate enough solution with a numerical error of about 2%. A Matlab program named SAS is written to facilitate the numerical computation and is available from the authors upon request, where SAS stands for a Stream-Aquifer-Stream system.

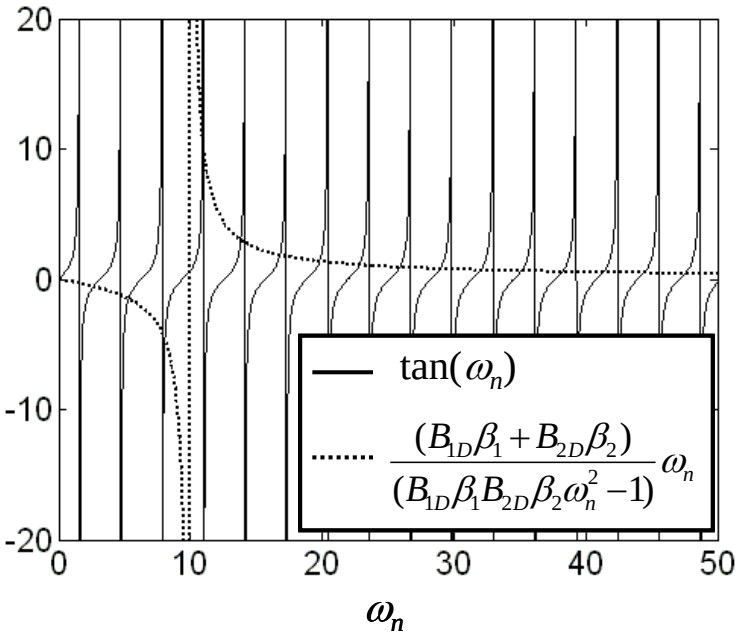

Figure 3.4 The diagram showing the solution of Eq. (C13). The solid and dashed lines represent the left and right hand sides of Eq. (C13) as functions of ω_n.

3.5 Results and Discussion

In this section, we will use some examples to illustrate the characteristics of capture zone between two streams for cases with and without the low-permeability streambeds. In the following discussion, the aquifer thickness is 30 m, the two parallel streams are 2000 m apart, and the regional flow is q=0.01m/d.

3.5.1 Capture zone between two streams without low-permeability streambeds

3.5.1.1 *Capture zone at the critical pumping rate*

As discussed in section 3.3.1, at the critical pumping rate, the stagnation point, S, is right at x_D=1 and y_D=0 (Figure 3.1, page 59). This is the circumstance that the capture

zone reaches its maximal size without extracting water from stream 2. Figure 3.5 shows the maximal capture zone at the critical pumping rate when the well is located at a=1500m or a_D=0.75, where line AB is the section of stream 1 intercepted by the envelope of the capture zone. The normalized critical pumping rate for this case is calculated to be 0.132 according to Eq. (3.9), which corresponds to a dimensional pumping rate of 497m^3/d. The value of the streamline AS is $\psi_D^s = \pi Q_{cD}$. Therefore, the y_D coordinate of the upper intercept point between the envelope of the capture zone and stream 1 can be determined by substituting the critical pumping rate into Eq. (3.6) and setting x_D=0 and $\psi_D^s = \pi Q_{cD}$

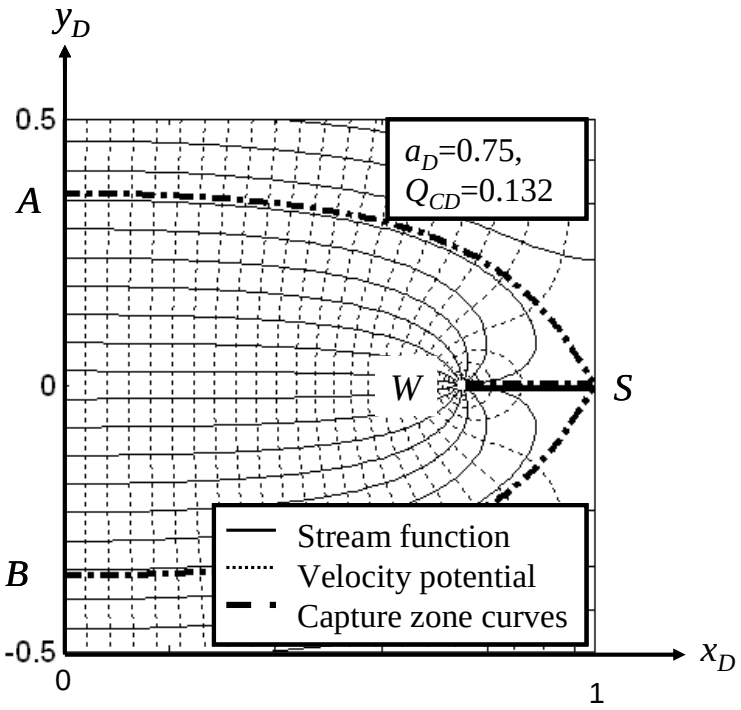

Figure 3.5 Flow net and envelope of the capture zone for the critical pumping case in which a single stagnation point is located at the intercept of the x-axis and stream 2. a_D is the normalized well location, and Q_{cD} is the corresponding normalized critical pumping rate. Low-permeability streambeds are not present.

$$\frac{\cot(\pi a_D/2)}{\pi}\tan^{-1}\left[\frac{\sin(\pi a_D)\sinh(\pi y_D)}{\cos(\pi a_D)\cos(\pi y_D)+1}\right]-y_D=\cot(\pi a_D/2), \tag{3.26}$$

An explicit solution for y_D is often unlikely, and we use a numerical root searching method such as the bisection or Newton-Raphson method to calculate y_D (Press et al., 1989). The point A can also be found graphically by plotting the streamlines using the Matlab program SAS.

It is also interesting to see how the maximal capture size from stream 1 varies with the location of the pumping well. Figure 3.6 shows the normalized maximal capture size which is the distance of AB in Figure 3.5 divided by *L*, as a function of the normalized well location a_D varying over a range of 0.5 to 0.9. The corresponding normalized critical pumping rate varies from 0.318 to 0.050. It is interesting to see that the maximal capture size decreases with a_D in an approximately linear fashion. Such a relationship is of great importance in terms of water management because one can estimate the maximal size of the capture zone for any given well location at the critical pumping rate.

The well only captures water from stream 1 when the pumping rate is less than the critical rate; whereas the well captures water from both streams when the pumping rate is greater than the critical rate. The latter case is of more interest to us from a water management perspective because one can compare the percentages of water extracted from two streams. Thus we will focus on this case in the following discussion.

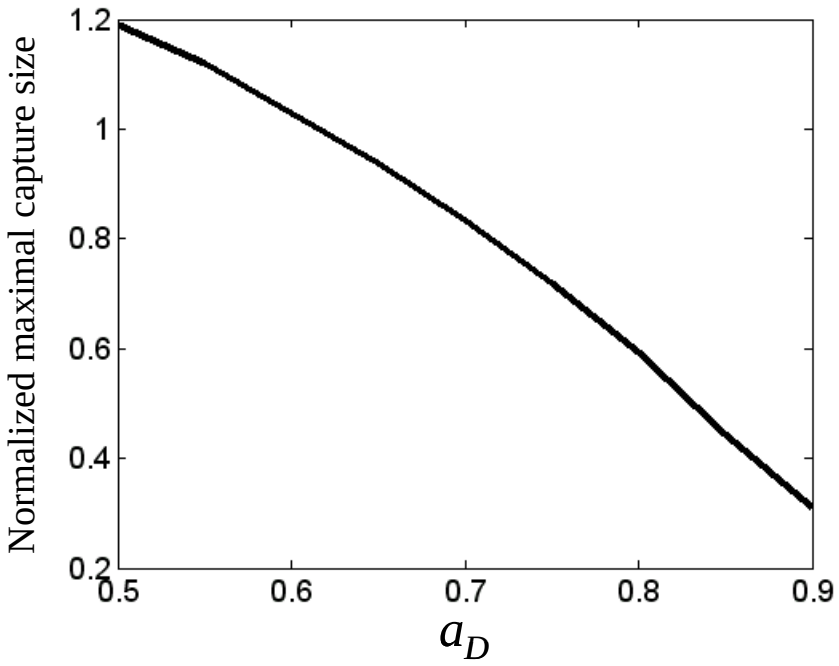

Figure 3.6 The normalized maximal capture zone without extracting water from the down-gradient stream versus the normalized well location, where the normalized maximal capture zone is defined by the ratio of the length of AB over the distance between two streams. Low-permeability streambeds are not present.

3.5.1.2 *Capture zone when the pumping rate is greater than the critical rate*

For this case, there are two stagnation points located at the x_D=1 and the coordinates of those stagnation points are obtained from Eq. (3.10). Figure 3.7 shows the flow net and the capture zone of this case for a_D=0.9 and Q_D=0.05. In this figure, AB and CD are the intercepted reaches of stream 1 and stream 2 respectively, where C and D are the two stagnation points; and W is the well location. The streamline values of AC and CW are ψ_{1D}^s and ψ_{2D}^s, respectively. The streamline values of BD and DW are -ψ_{1D}^s and -ψ_{2D}^s because of the symmetry of the capture zone. The ψ_{1D}^s can be found from

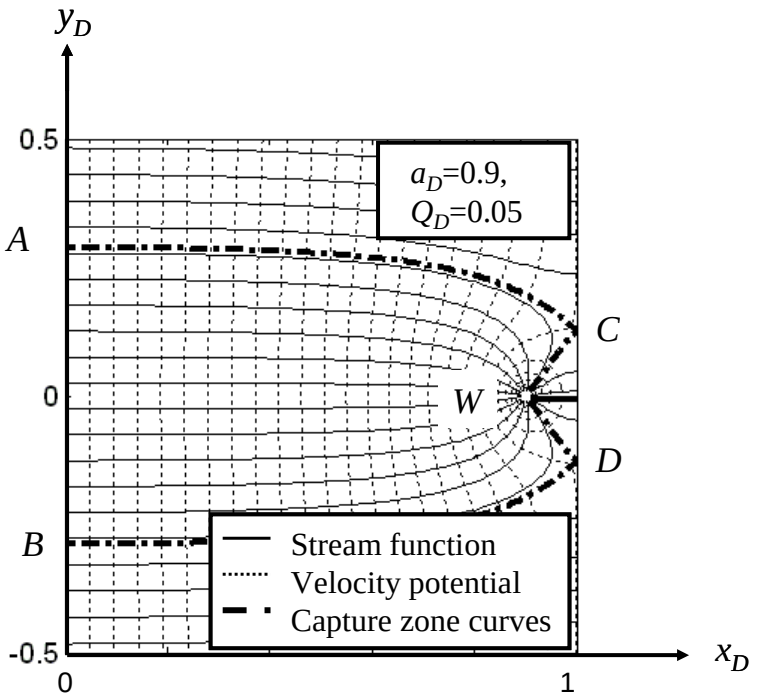

Figure 3.7 Flow net and the envelope of the capture zone when the pumping rate is greater than the critical pumping rate. Two stagnation points located at stream 2 are found. Low-permeability streambeds are not present.

Eq. (3.6) by letting x_D=1 and $y_D \to y_{0D}^{+}$, where $y \to y_{0D}^{+}$ means approaching the stagnation point from the side of $y > y_{0D}$ (curve AC). Similarly, ψ_{2D}^{s} can be found from Eq. (3.6) by letting x_D=1 and $y_D \to y_{0D}^{-}$, where $y \to y_{0D}^{-}$ means approaching the stagnation point from the side of $y < y_{0D}$ (curve CW). The pumping induced depletions from stream 1 and stream 2 are proportional to $2\psi_{1D}^{s}$ and $2\psi_{2D}^{s}$, respectively**.** Therefore, the ratio of pumping induced depletions from stream 1 and stream 2 becomes

$$Q_{1D} / Q_{2D} = \psi_{1D}^{s} / \psi_{2D}^{s}. \qquad (3.27)$$

Since $Q_{1D} + Q_{2D} = Q_D$, one has

$$Q_{1D} = Q_D \psi_{1D}^s / (\psi_{1D}^s + \psi_{2D}^s),\ Q_{2D} = Q_D \psi_{2D}^s / (\psi_{1D}^s + \psi_{2D}^s). \quad (3.28)$$

Figure 3.8 shows the normalized flux from stream 1, Q_{1D} / Q_D, as a function of the normalized well location for three various normalized pumping rates of 0.133, 0.265, and 1.326. The other normalized flux, Q_{2D} / Q_D, can be easily derived from this figure based on Eq. (3.28). A number of points can be observed from Figure 3.8. First, this figure shows that the normalized flux decreases with a_D faster than the linear fashion, meaning that the magnitude of the slope of the curve increases with a_D. Second, a larger Q_D will lead to a smaller normalized flux from stream 1 at a given well location a_D. Third, when Q_D is larger, the pumping well will start to extract water from stream 2 at a much smaller a_D, reflected by the early departure of the curve from the upper horizontal axis in Figure 3.8. Since the aquifer thickness and the distance between the streams are fixed in this calculation, Q_D is directly related to Q / q, and a larger Q_D implies that the pumping rate is relatively greater than the regional flow and vice versa.

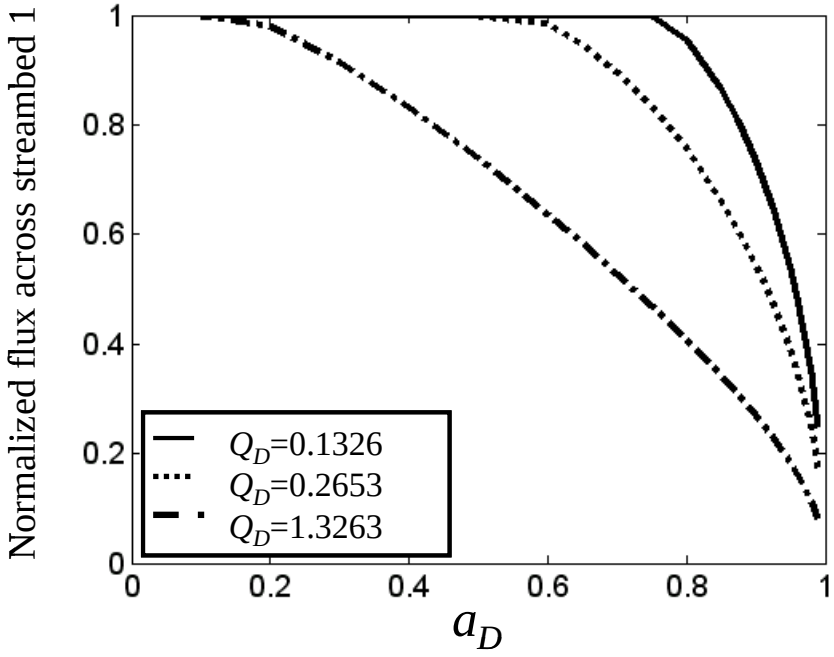

Figure 3.8 The normalized flux across stream 1 versus the normalized well location for three normalized pumping rates. Low-permeability streambeds are not present.

3.5.2 Capture zone between two streams with low-permeability streambeds

For this case, we use the same default values as in the case without streambeds, i.e., a 30m thick aquifer bounded by two parallel streambeds at a distance of 2000m, except that q is assumed to be zero here. Two primary factors governing flux across a streambed are the hydraulic conductivity and the thickness of the streambed. These two properties are lumped into a hydraulic conductance defined as $C_1=K_1/B_1$ and $C_2= K_2/B_2$ for streambed 1 and streambed 2, respectively. The hydraulic conductance of the aquifer is defined as $C=K/L$ here. Notice that the thickness of the streambed is often at the sub-

meter scale and the hydraulic conductivity values of the streambeds are at least two orders of magnitude smaller than that of the aquifer, thus the hydraulic conductance of the streambed might be smaller, equal, or greater than that of the aquifer, depending on the field situations (Cardenas and Zlotnik, 2003; Chen and Chen, 2003a, 2003b).

Figure 3.9 shows the normalized fluxes across streambed 1 as functions of the normalized well location for C_1/C_2 of 0.1, 1, and 10, respectively. C_2/C is fixed to be 1 and Q is 500m^3/d in Figure 3.9. A number of interesting points have been observed from this figure. First, all three cases in Figure 3.9 show nearly linear decrease of flux across streambed 1 over a_D. This is somewhat different from Figure 3.8 when the regional flow is present. It appears that existence of the regional flow will result in curved streamlines in the aquifer to the pumping well, leading to that the flux from streambed 1 decreases over a_D slower than the linear rate. When the regional flow does not exist, streamlines in the aquifer are straight to the pumping well, leading to a linear decrease of flux from streambed 1 over a_D. Second, when C_1/C_2 equals one, the magnitude of the slope of the flux versus a_D is nearly unity. Third, for the cases of C_1/C_2 equaling 0.1 and 10, the magnitudes of slopes of the flux versus a_D are nearly identical, and are less than unity. For example, the magnitudes of slopes for the cases of C_1/C_2 equaling 0.1 and 10 are approximately 0.6 in Figure 3.9. This indicates that the slope of the curve is governed by the ratio of C_1/C_2. Similar conclusions can be drawn for fluxes from streambed 2. A greater ratio of C_1/C_2 indicates easier withdrawal of water from stream 1 for a given a_D. For example, when a_D = 0.1, 38.8%, 12.5%, and 9.3% of

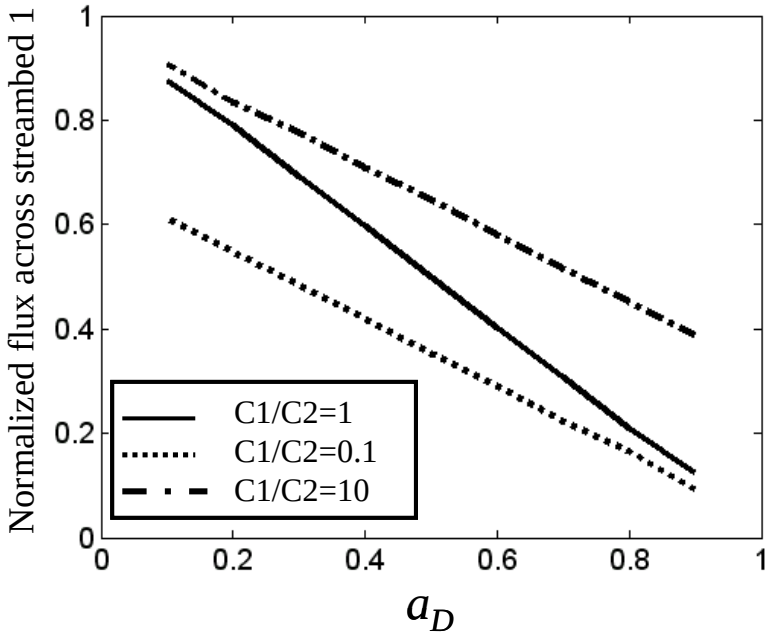

Figure 3.9 The normalized flux across streambed 1 versus the normalized well location for C_1/C_2 equaling 0.1, 1, and 10, respectively. C_1 and C_2 are the hydraulic conductances of the streambeds 1 and 2, respectively.

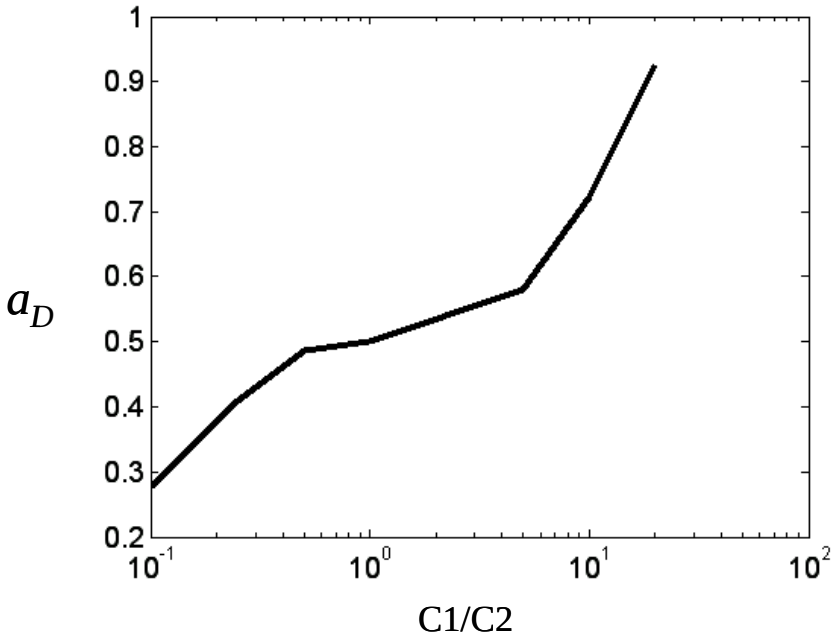

Figure 3.10 The normalized well location versus C_1/C_2 under the condition that fluxes across streambeds 1 and 2 are equal. C_1 and C_2 are the hydraulic conductances of the streambeds 1 and 2, respectively.

extracted water come from stream 1 for the cases of C_1/C_2 equaling 10, 1, and 0.1, respectively.

Figure 3.10 shows the normalized well location with equal fluxes from stream 1 and stream 2 versus various ratio of C_1/C_2 for a fixed Q of 500m^3/d in a semi-log plot. When C_1/C_2 is less than unity, a_D must be closer to stream 1 to obtain equal fluxes from both streams because it is harder for water to flow across streambed 1. It is interesting to observe that the increase of a_D versus C_1/C_2 follows a three-segment development including a steep segment at the beginning, followed by a flat segment and a final steep segment.

The three-segment curve shown in Figure 3.10 implies a few features of streambed influence on stream depletion. When the values of hydraulic conductance of the two streambeds are off by more than an order of magnitude, the stream depletion is quite sensitive to the well location which has to be sufficiently close to the streambed with the lower hydraulic conductivity for extracting equal flows from both streams. This corresponds to the first and the third steep segments of Figure 3.10. On the other hand, if the values of hydraulic conductance of the two streambeds are more or less the same, or off by less than an order of magnitude, the stream depletion becomes less sensitive to the dimensionless well location which is around 0.5 for extracting equal flows from both streams. This corresponds to the middle flat segment of Figure 3.10.

3.6 Summary and Conclusions

We have developed semi-analytical method to calculate the stream depletion in an aquifer bounded by two parallel streams with and without any streambeds. In the

case without any streambeds, we have performed capture zone analysis and presented the normalized maximal capture size from the up-gradient stream without extracting water from the down-gradient stream as a function of the normalized well location (Figure 3.6). This diagram can be used to determine maximum capture zone size. We have also presented the normalized flux entering the aquifer as a function of the normalized well location for three different normalized pumping rates in the case without any streambeds (Figure 3.8). For the aquifer with streambeds, we have presented the normalized flux as a function of the normalized well location for three different combinations of hydraulic conductances (Figure 3.9). Furthermore, the normalized well location for a well that receives equal fluxes from two streams as a function of different streambed hydraulic conductance ratios is also provided (Figure 3.10). We can draw the following conclusions from this study.

The hydraulic conductances of the low-permeability streambeds are probably the most important parameters affecting the capture zones.

When the low-permeability streambeds are not present, the maximal capture size without extracting water from the down-gradient stream decreases with the normalized well location (a_D) in an approximately linear fashion. The normalized flux from the up-gradient stream decreases with the normalized well location faster than the linear fashion, meaning that the magnitude of the slope of the curve increases with a_D.

When the streambeds exist and the regional flow is neglected, the normalized flux across the up-gradient streambed varies with the normalized well location in a linear fashion. The magnitude of the slope of the normalized flux across the up-gradient

streambed versus the normalized well location is nearly unity when the hydraulic conductance ratio of the two streambeds is one; and the magnitude of such a slope is less than unity when the hydraulic conductance ratio of the two streambeds is either greater or smaller than one. If the normalized well location for a well receiving equal fluxes from two streams versus the hydraulic conductance ratio of the two streambeds is plotted semi-logarithmically, one will observe a three-segment trend including a steep segment at the beginning, followed by a flat segment and a final steep segment.

CHAPTER IV

SUMMARY AND FUTURE WORKS

4.1 Summary

In this dissertation, we have investigated stream aquifer interaction focusing on stream depletion rates of various settings. We have also studied hydraulic parameters affecting the stream depletion rates. Solutions for drawdown in the aquifers for each case are presented. Capture zone analysis is performed for a pumping well in the aquifer between two streams.

Chapter II considers drawdown and stream depletion caused by a fully penetrating pumping well near a fully penetrating stream with and without the streambed. General solutions of drawdown in the aquifer in the Laplace-Fourier domain with and without streambeds for any pumping schedules and any stream stage functions are presented. We consider two general stream stage functions. For the seasonal fluctuation case, the stream stage is a function of time only. For the short-term fluctuation case, the stream stage depends on time and distance along the stream. The following function: $h_S(t) = A\left(1 - \cos(\omega t)\right)$ is used to describe the seasonal stream stage variation. We present semi-analytical stream depletion rates (in time domain) using a numerical method to solve for stream depletion caused by stream stage fluctuations and using an analytical method to solve for stream depletion caused by a pumping well for both with and without streambed sediments.

Three primary factors affecting the stream depletion caused by stream fluctuations are the pumping rate, the frequency of the flood, and the stream length that

is used to evaluate the stream depletion. The period of stream fluctuation plays a crucial role in affecting the stream depletion. A shorter period yields a grater rate of stream depletion caused by stream stage fluctuation.

If a streambed exist, it can greatly reduce stream depletion caused by stream stage fluctuations; however, when pumping time is long enough, the stream depletion rate caused by the extraction well is insensitive to the streambed parameters.

For the short-term floodwave fluctuation, general solutions of drawdown in the aquifer in the Laplace-Fourier domain with and without streambed for any pumping schedules and any stream stage functions are presented. The following function: $h_S(y,t) = \frac{A_0}{2\sqrt{\pi D t}} e^{-\frac{(y-vt)^2}{4Dt}}$ is used to describe the short-term stream stage fluctuations. An analytical stream stage depletion rate in real time domain is presented for the case without the streambed. The stream depletion rate for the case with the streambed is solved in the same manner as the seasonal fluctuation case.

We have derived the analytical solutions of the stream depletion rates at early and late times caused by stream fluctuation following a cosine function. It is interesting to point out that the late time stream depletion decays with time as a fashion that is inversely proportional to the square root of time. This implies that the stream depletion caused by stream stage fluctuation can be neglected for a stream aquifer system that has years to equilibrate. At late times, the pumping well becomes the dominating factor for influencing the stream depletion. At early time, however, the contributions from both the stream stage fluctuation and the pumping well have to be considered.

The drawdown and stream depletion rate can be written in two separated terms and can be solved independently. If one would like to add additional component, it can be done by superposition another term in the existing result.

In Chapter III, we have developed semi-analytical method to calculate the stream depletion in an aquifer bounded by two parallel streams with and without any streambeds. In the case without any streambeds, we have performed capture zone analysis and presented the normalized maximal capture size from the up-gradient stream without extracting water from the down-gradient stream as a function of the normalized well location (Figure 3.6). This diagram can be used to determine maximum capture zone size. We have also presented the normalized flux entering the aquifer as a function of the normalized well location for three different normalized pumping rates in the case without any streambeds (Figure 3.8). For the aquifer with streambeds, we have presented the normalized flux as a function of the normalized well location for three different combinations of hydraulic conductances (Figure 3.9). Furthermore, the normalized well location for a well that receives equal fluxes from two streams as a function of different streambed hydraulic conductance ratios is also provided (Figure 3.10). We can draw the following conclusions from this study.

The hydraulic conductances of the low-permeability streambeds are probably the most important parameters affecting the capture zones.

When the low-permeability streambeds are not present, the maximal capture size without extracting water from the down-gradient stream decreases with the normalized well location (a_D) in an approximately linear fashion. The normalized flux from the up-

gradient stream decreases with the normalized well location faster than the linear fashion, meaning that the magnitude of the slope of the curve increases with a_D.

When the streambeds exist and the regional flow is neglected, the normalized flux across the up-gradient streambed varies with the normalized well location in a linear fashion. The magnitude of the slope of the normalized flux across the up-gradient streambed versus the normalized well location is nearly unity when the hydraulic conductance ratio of the two streambeds is one; and the magnitude of such a slope is less than unity when the hydraulic conductance ratio of the two streambeds is either greater or smaller than one. If the normalized well location for a well receiving equal fluxes from two streams versus the hydraulic conductance ratio of the two streambeds is plotted semi-logarithmically, one will observe a three-segment trend including a steep segment at the beginning, followed by a flat segment and a final steep segment.

4.2 Future Works

A long term goal of this study is to implement these solutions to a GIS based model which includes other hydrological data to do real time calculation for suitable pumping rates to sustain the hydrological and ecological system.

In Chapter II, a section of stream used to evaluate the total seasonal stream depletion is a constant with an arbitrary value. Substituting this value with capture zone size of the pumping well would yield more accurate results. For a short-term case, finding a better function to simulate flood wave or solving the dynamic floodwave model is the next step.

In Chapter III, we assume stream stages are constant. Allowing the stream stage to fluctuate would represent a more realistic case. Comparing issues such as partial penetration or size of stream of stream-aquifer-stream system to a steam aquifer system would be interesting.

REFERENCES

Ahlfeld, D.P., Sawyer, C.S., 1990. Well location in capture zone design using simulation and optimization techniques. Ground Water 28 (4), 507–512.

Akan, A.O., 2006. Open Channel Hydraulics. Butterworth-Heinemann, Oxford, UK, 336-337

Akylas, E., Koussis, A.D., 2007. Response of sloping unconfined aquifer to stage changes in adjacent stream. I. Theoretical analysis and derivation of system response functions. J. Hydrol. 338, 85-95.

Arfken, G.B., Weber, H.J., 1995. Mathematical Method for Physicists, 4th ed. Academic, San Diego, CA.

Bair, E.S., Roadcap, G.S., 1992. Comparison of flow models used to delineate capture zones of wells: 1. Leaky-confined fractured carbonate aquifer. Ground Water 30 (2), 199–211.

Barlow, P.M., Monech, A.F. ,1998. Analytical solutions and computer programs for hydraulic interaction of stream-aquifer systems. US geological Survey Open-File Report 98-415 A, PP 85.

Bear, J., 1972. Dynamics of Fluids in Porous Media. Elsevier, New York.

Bear, J., 1979. Hydraulics of Ground Water. McGraw-Hill, New York.

Bruggeman, G. A., 1999. Analytical Solutions of Geohydrological Problems. Elsevier, Amsterdam, The Netherlands.

Butler, J.J., Zlotnik, V.A., Tsou, M.S. 2001. Drawdown and stream depletion produced by pumping in the vicinity of a finite width stream of shallow penetration. Ground Water 39(5), 651-659.

Cardenas, M.B., Zlotnik, V.A., 2003. Three dimensional model of modern channel bend deposites. Water Resour. Res. 39 (6), 1141, doi:10.1029/2002WR001383.

Chanson, H., 2004. Environmental hydraulics of open channel flows. Elsevier, Burlington, MA.

Chen, X.H., Chen, X., 2003a. Sensitivity analysis and determination of streambed leakance and aquifer hydraulic properties. J. Hydrol. 284, 270-284.

Chen, X.H., Chen, X., 2003b. Effects of aquifer anisotropy on the migration of infiltrated stream water to a pumping well. J. Hydrol. Eng. 8 (5), 287-293.

Chen, X., Yin, Y., 2001. Streamflow depletion: Modeling of reduced baseflow and induced stream infiltration from seasonally pumped wells. J. Am. Water Resour. Assoc. 37, 185-195.

Chow, V.T., 1959. Open Channel Flow. Prentice-Hall, Englewood Cliffs, NJ.

Christ, J.A., Goltz, M.N., 2002. Hydraulic containment: analytical and semi-analytical models for capture zone curve delineation. J. Hydrol. 262, 224–244.

Conrad, L.P., Beljin, M.S., 1996. Evaluation of an induced infiltration model as applied to glacial aquifer systems. J. Amer. Water Resources Association 32 (6), 1209-1220.

Cooper, H.H., Jr., Rorabaugh, M.I., 1963. Ground-water movements and bank storage caused by flood stages in surface stream: U.S. Geological Survey Water-Supply Paper 1536-J, 343-366

Cunningham, J.A., Hoelen, T.P., Hopkins, G.D., Lebrón, C.A., Reinhard, M., 2004. Hydraulics of recirculating well pairs for ground water remediation. Ground Water 42 (6), 880-889.

de Hoog, F.R., Knight, J.H., Stokes, A.N., 1982. An improved method for numerical inversion of Laplace transforms. S.I.A.M. J. Sci. and Stat. Comput., 3, 357-366.

Faybishenko, B.A., Javandel, I., Witherspoon, P.A., 1995. Hydrodynamics of the capture zone of a partially penetrating well in a confined aquifer. Water Resour. Res. 31 (4), 859–866.

Glover, R.E., Balmer, C.G., 1954. River depletion resulting from pumping a well near a river. Eos. Trans. Am. Geophys. Union 35, 468-470.

Granato, G.E., Barlow, P.M., 2004. Criteria and Water-Supply Demands on Ground-Water Development Option in the Big River Area, Rhode Island. US Geological Survey Scientific Investigation Report. 5301.

Grubb, S., 1993. Analytical model for estimation of steady-state capture zones of pumping wells in confined and unconfined aquifers. Ground Water 31 (1), 27–32.

Hantush, M.S., 1965. Wells near streams with semipervious beds. J. of Geophys. Res. 70, 2829-2838

Hantush, M.M., 2005. Modeling stream aquifer interaction with linear response functions. J. Hydrol. 311, 59-79.

Hollenbeck, K. J., 1998. INVLAP.M: A matlab function for numerical inversion of Laplace transforms by the de Hoog algorithm, http://www.isva.dtu.dk/staff/karl/invlap.htm

Hunt, B., 1999. Unsteady stream depletion from ground water pumping, Ground Water 37(1), 98-102.

Intaraprasong, T., Zhan H., 2007. Capture zone between two streams, J. Hydrol. 338, 297-307, 2007

Javandel, I., Tsang, C.F., 1986. Capture zone type curves: a tool for aquifer cleanup. Ground Water 24 (5), 616–625.

Jenkins, C.T., 1968. Techniques for computing rate and volume of stream depletion by wells. Ground Water 6, 37-46.

Jenkins, C.T., 1970. Computation of rate and volume of stream depletion by wells: Techniques of Water-Resources Investigations of the U.S. Geological Survey, U.S. Department of the Interior, Ch.D1, 1-17.

Kim, K.Y., Kim, T., Kim, Y., Woo, N.C., 2007. A semi-analytical solution for groundwater response to stream-stage variations and tidal fluctuations in a coastal aquifer. Hydrological Processes 21(5), 665-674.

Kirk, S., Herbert, A.W., 2002, Assessing the impact of groundwater abstractions on river flows. Geological Society, London, Special Publications 193, 211-233, doi: 10.1144/GSL.SP.2002.193.01.16.

Kollet, S.J., 2005. Comment on “Sensitivity analysis and determination of streambed leakance and aquifer hydraulic properties” by Xunhong Chen and Xi Chen, 2003. J. Hydrol. 284, 270-284. J. Hydrol. 303, 328-330.

Kollet, S.J., Zlotnik, V.A., 2003. Stream depletion predications using pumping test data from a heterogeneous stream-aquifer system (a case study from the Great Plains, USA), J. Hydrol. 281, 96-114.

Kompani-Zare, M., Zhan, H., Samani, N., 2005. Analytical study of capture zone to a horizontal well in a confined aquifer. J. Hydrol. 307 (1-4), 48-59.

Larkin, R.G., Sharp, J.M. 1992. On the relationship between river-basin geomorphology, aquifer hydraulics, and groundwater flow direction in alluvial aquifers. GSA Bulletin 104 (12), 1608-1620.

Lerner, D.N., 1992. Well catchments and time of travel zones in aquifers with recharge. Water Resour. Res. 28 (10), 2621–2628.

Loheide, S.P., II, Butler, J.J., Jr., and Gorelick, S.M., 2005, Estimation of groundwater consumption by phreatophytes using diurnal water table fluctuations: A saturated-unsaturated flow assessment: Water Resour. Res., 41, W07030, doi:10.1029/2005WR003942

Luo, J., Kitanidis, P.K., 2004. Fluid residence times within a recirculation zone created by an extraction-injection well pair. J. Hydrol. 295 (1-4), 149-162.

Moench, A.F., Barlow, P.M., 2000. Aquifer response to stream-stage and charge variations. I. Analytical step-response functions, J. Hydrol. 230, 192-210.

Muskat, M., 1946. The Flow of Homogeneous Fluids through Porous Media. J.W. Edwards, Ann Arbor, MI.

Newsom, J.M., Wilson, J.L., 1998. Flow of ground water to a well near a stream—effect of ambient ground-water flow direction. Ground Water 26 (6), 703-711.

Polubarinova-Kochina, P.Y., 1962. Theory of Ground Water Movement. Princeton University Press, Princeton, NJ.

Press, W.H., Flannery, B.P., Teukolsky, S.A., Vetterling, W.T., 1989. Numerical Recipes, the Art of Scientific Computing (FORTRAN Version). Cambridge Univ. Press, NY.

Prudic, D.E., 1989. Documentation of a computer program to simulate stream-aquifer relations using a modular, finite-difference, ground-water flow model. U.S. Geological Survey Open-File Report 88-729. Carson City, NV, 113.

Rorabaugh, M.I., 1963. Streambed percolation in development of water supplies. US Geological Survey Water Supply Paper 1554H, H47-H62.

Rutschman, P., Hager, W.H., 1996. Diffusion of floodwaves, J. of Hydrol. 178, 19–32.

Schafer, D.C., 1996. Determining 3D capture zones in homogeneous, anisotropic aquifers. Ground Water 34 (4), 628–639.

Serrano, S.E., Workman, S.R., 1998. Modeling transient stream–aquifer interaction with the nonlinear Boussinesq equation and its analytical solution. J. Hydrol. 206, 245–255.

Shafer, J.M., 1987. Reverse path line calculation of time-related capture zones in nonuniform flow. Ground Water 25 (3), 283–289.

Shan, C., 1999. An analytical solution for the capture zone of two arbitrarily located wells. J. Hydrol. 222 (1–4), 123–128.

Singh, S.K., 2004. Ramp kernels for aquifer responses to arbitrary stream stage, J. of Irrigation and Drainage Engineering. 103, 460-467.

Sophocleous, M.A., Koussis, A., Martin, J.L., and Perkins, S.P., 1995. Evaluation of simplified stream-aquifer depletion models for water rights administration. Ground Water 33, 579-588.

Spalding, C.P., Khaleel, R., 1991. An evaluation of analytical solutions to estimate drawdown and stream depletion by wells, Water Resour. Res. 27**,** 597–609.

Steward, D.R., 1999. Three-dimensional analysis of the capture of contaminated leachate by fully penetrating, partially penetrating, and horizontal wells. Water Resour. Res. 35 (2), 461–468.

Sun, D., Zhan, H., 2006. Flow to a horizontal well in an aquifer-aquitard system. J. Hydrol. 321, 364-376.

Sun, D., Zhan, H., 2007. Pumping induced depletion from two streams. Adv. Water Resour. 30(4), 1016-1026.

Theis, C.V., 1941. The effect of a well on the flow of a nearby stream. Eos Trans., Am. Geophys. Union 22, 734-738.

Tiedeman, C., Goreick, S.M., 1993. Analysis of uncertainty in optimal groundwater contaminant capture design. Water Resour. Res. 29 (7), 2139–2153.

Wallace, R.B., Darama, Y., Anneable, M.D., 1990. Stream depletion by circle pumping of wells. Water Resour. Res. 26(6), 1263-1270.

Wilson, J.L., 1993. Induced infiltration in aquifer with ambient flow. Water Resour. Res. 29 (10), 3503–3512.

Winter, T.C., Harvey, J.W., Frank, O.L., Alley, W.M., 1998. Ground water and surface water a single resource. US Department of the Interior, Geological Survey Circular 1139.

Woessner, W.W., 2000. Stream and fluvial plain ground water interactions: Rescaling hydrogeologic thought, Ground Water 38 (3), 423-429.

Wurster, F.C., Cooper, D.J., Sanford, W.E., 2003. Stream/aquifer interactions at Great Sand Dunes National Monument, Colorado: influences on interdunal wetland disappearance. J. Hydrol., 271(1-4), 77-100.

Zhan, H., 1999a. Analytical and numerical modeling of a double-well capture zone. Mathematical Geology 31 (2), 175-193.

Zhan, H., 1999b. Analytical study of capture time to a horizontal well. J. Hydrol. 217, 46-54.

Zhan, H., Cao, J., 2000. Analytical and semi-analytical solutions of horizontal well capture times under no-flow and constant –head boundaries, Adv. Water Resour., 23(8), 835-848.

Zhan, H., Park, E., 2003. Hydraulics of horizontal wells in leaky aquifers, J. Hydrol. 281, 133-150.

Zhan H., Wang, L.V., Park, E., 2001. On the horizontal-well pumping tests in anisotropic confined aquifer, J. Hydrol. 252, 37-50.

Zhan, H., Zlotnik, V.A., 2002. Ground water flow to horizontal and slanted wells in unconfined aquifers, Water Resour. Res., doi: 10.1029/2001WR000401.

Zhang, D.X., Lu, Z.M., 2004. Stochastic delineation of well capture zones. Stochastic Environmental Research and Risk Assessment 18 (1), 39-46.

Zlotnik, V.A., 2004. A concept of maximum stream depletion rate for leaky aquifers in alluvial valleys. Water Resour. Res. 40, W06507, doi:10.1029/2003WR002932

Zlotnik, V.A., Huang, H., 1999. Effect of shallow penetration and streambed sediments on aquifer response to stream stage fluctuations (analytical model). Ground water 37(4), 599-605.

Zlotnik, V. A., Huang, H., Butler, J.J., 1999. Evalution of stream depletion considering finite stream width, shallow penetration, and properties of streambed sediments. In Proceeding of Water 99, Joint Congress, Brisbane, Australia, 221-226.

Zlotnik, V.A., Zhan, H., 2005. The aquitard effect on drawdown in water table aquifers, Water Resour. Res. 41 (6), W06022, doi: 10.1029/2004WR003716

APPENDIX A

Appendix A show detailed derivation of $\bar{\bar{s}}_D$ of the system without any streambed. Converting heads to drawdown, converting variables to dimensionless variables, and apply Laplace transform to Eqs. (2.1) to (2.4), one obtains

$$p\bar{s}_D = \frac{\partial^2 \bar{s}_D}{\partial x_D^2} + \frac{\partial^2 \bar{s}_D}{\partial {y_D}^2} + 4\pi\overline{Q}_D(p)\delta(x_D - x_{wD})\delta(y_D) \tag{A1}$$

$$\bar{s}_D(x_D, y_D, t_D = 0) = 0 \tag{A2}$$

$$\bar{s}_D(x_D = 0, y_D, t_D) = \overline{H}_{SD}(p) \tag{A3}$$

Conducting Fourier transform along *y*-axis to Eq. (A1),

$$\frac{\partial^2 \bar{\bar{s}}_D}{\partial x_D^2} - (p + f_y^2)\bar{\bar{s}}_D + 4\pi\overline{Q}_D(p)\delta(x_D - x_{wD}) = 0 \tag{A4}$$

General solutions of Eq. (A4) are

$$\bar{\bar{s}}_D = c_1 \cosh[\sqrt{\beta}x_D] + c_2 \sinh[\sqrt{\beta}x_D], \text{ for } 0 \le x_D \le x_{WD} \tag{A5}$$

$$\bar{\bar{s}}_D = c_3 e^{-\sqrt{\beta}x_D}, \text{ for } x_{WD} < x_D \tag{A6}$$

where $\beta = p + f_y^2$.

Conducting Fourier transform to Eq. (A3), the result is

$$\bar{\bar{s}}_D(x_D = 0, y_D, t_D) = \overline{H}_{SD}(p)\delta(f_y)2\pi = \hat{\overline{H}}_{SD} \tag{A7}$$

From evaluation Eq. (A5) at $x_D = 0$ and set it equal to Eq. (A7), one obtains

$$c_1 = \hat{\overline{H}}_{SD} \tag{A8}$$

Drawdown should be continuous at the well, $x_D = x_{WD}$, evaluate Eqs.(A5) and (A6) at the well and set them equal to each other,

$$c_1 \cosh(\sqrt{\beta} x_{WD}) + c_2 \sinh(\sqrt{\beta} x_{WD}) = c_3 e^{-\sqrt{\beta} x_{WD}} \tag{A9}$$

The first divertive of drawdown is discontinuous at $x_D = x_{WD}$. Taking integration of Eq. (A4) from $x_{WD} - dx$ to $x_{WD} + dx$, where *dx* is an infinitely small interval, the result is

$$\left.\frac{\partial^2 \bar{\bar{s}}_D}{\partial x_D^2}\right|_{x_{WD}+dx} - \left.\frac{\partial^2 \bar{\bar{s}}_D}{\partial x_D^2}\right|_{x_{WD}-dx} + 4\pi \bar{Q}_D = 0 \tag{A10}$$

Substitute Eqs. (A5) and (A6) into Eq. (A10),

$$-\sqrt{\beta} c_3 e^{-\sqrt{\beta} x_{WD}} - \left[\sqrt{\beta} c_1 \sinh(\sqrt{\beta} x_{WD}) + \sqrt{\beta} c_2 \cosh(\sqrt{\beta} x_{WD})\right] + 4\pi \bar{Q}_D = 0 \tag{A11}$$

Solving Eqs. (A9) and (A11) for c_2 and c_3, the results are

$$c_2 = -\hat{\bar{H}}_{SD} + \frac{4\pi}{\sqrt{\beta}} \bar{Q}_D e^{-\sqrt{\beta} x_{WD}} \tag{A12}$$

$$c_3 = \hat{\bar{H}}_{SD} + \frac{4\pi}{\sqrt{\beta}} \bar{Q}_D \sinh(\sqrt{\beta} x_{WD}) \tag{A13}$$

Substituting c_1, c_2, and c_3 into Eqs. (A5) and (A6), the drawdown in the aquifer is show in Eqs. (2.5) and (2.6).

APPENDIX B

Appendix B shows detailed derivation of $\bar{\bar{s}}_D$ of the system with streambeds. Converting heads to drawdown, converting variables to dimensionless variables, and Laplace transforming Eqs. (2.16), (2.17), (2.18), (2.19), and (2.21), one obtains

$$\mu p \bar{s}_D' = \frac{d^2 \bar{s}_D'}{dx_D^2} \tag{B1}$$

$$\bar{s}_D'(x_D = -B_D') = \bar{H}_{SD} \tag{B2}$$

$$p\bar{s}_D = \frac{\partial^2 \bar{s}_D}{\partial x_D^2} + \frac{\partial^2 \bar{s}_D}{\partial {y_D}^2} + 4\pi \bar{Q}_D(p)\delta(x_D - x_{wD})\delta(y_D) \tag{B3}$$

$$\bar{s}_D'(x_D = 0, y_D) = \bar{s}_D(x_D = 0, y_D) \tag{B4}$$

$$\lambda \left.\frac{\partial \bar{s}_D'}{\partial x_D}\right|_{x_D=0} = \left.\frac{\partial \bar{s}_D}{\partial x_D}\right|_{x_D=0} \tag{B5}$$

Solution of Eq. (B1) is

$$\bar{s}_D' = c_1 \cosh\left(\sqrt{\mu p}(x_D + B_D')\right) + c_2 \sinh\left(\sqrt{\mu p}(x_D + B_D')\right) \tag{B6}$$

Fourier transform to Eqs. (B3) to (B5)

$$\frac{\partial^2 \bar{\bar{s}}_D}{\partial x_D^2} - (p + f_y^2)\bar{\bar{s}}_D + 4\pi \bar{Q}_D(p)\delta(x_D - x_{wD}) = 0 \tag{B7}$$

$$\bar{\bar{s}}_D'(x_D = 0) = \bar{\bar{s}}_D(x_D = 0) \tag{B8}$$

$$\lambda \left.\frac{\partial \bar{\bar{s}}_D'}{\partial x_D}\right|_{x_D=0} = \left.\frac{\partial \bar{\bar{s}}_D}{\partial x_D}\right|_{x_D=0} \tag{B9}$$

Let $\beta = p + f_y^2$, the solutions of Eq. (B7) are

$$\bar{\bar{s}}_D = c_3 \cosh[\sqrt{\beta} x_D] + c_4 \sinh[\sqrt{\beta} x_D], \text{ for } 0 \le x_D \le x_{WD} \tag{B10}$$

$$\bar{\bar{s}}_D = c_5 e^{-\sqrt{\beta} x_D}, \text{ for } x_{WD} < x_D \tag{B11}$$

Substituting c_1 and c_2 into Eq. (B6), one obtains expressions for drawdown in the streambed in Fourier domain. Detailed derivation of c_1, c_2, c_3, c_4, and c_5 is shown below.

Fourier transform Eq. (B10),

$$\bar{\bar{s}}_D' = \bar{c}_1 \cosh\left(\sqrt{\mu p}(x_D + B_D')\right) + \bar{c}_2 \sinh\left(\sqrt{\mu p}(x_D + B_D')\right) \tag{B12}$$

Fourier transform Eq. (B2),

$$\bar{\bar{s}}_D'(x_D = -B_D') = \bar{\bar{H}}_{SD} = \bar{H}_{SD} \partial(f_y) \sqrt{2\pi} = \hat{\bar{H}}_{SD} \tag{B13}$$

Substitute $x_D = -B_D'$ in Eq. (B12) and set it equal to Eq. (B13), then

$$\bar{c}_1 = \hat{\bar{H}}_{SD} \tag{B14}$$

Evaluate Eqs. (B10) and (B11) with condition of Eq. (B8),

$$\bar{c}_3 = \hat{\bar{H}}_{SD} \cosh\left(\sqrt{\mu p} B_D'\right) + \bar{c}_2 \sinh\left(\sqrt{\mu p} B_D'\right) \tag{B15}$$

$$\sqrt{\beta}\bar{c}_4 = \lambda\left(\hat{\bar{H}}_{SD} \sqrt{\mu p} \sinh\left(\sqrt{\mu p} B_D'\right) + \bar{c}_2 \sqrt{\mu p} \cosh\left(\sqrt{\mu p} B_D'\right)\right) \tag{B16}$$

Now use continuity of drawdown at the well $\bar{\bar{s}}_D(x_D = x_{WD} - dx_D) = \bar{\bar{s}}_D(x_D = x_{WD} + dx_D)$

$$\bar{c}_3 \cosh\left(\sqrt{\beta} x_{WD}\right) + \bar{c}_4 \sinh\left(\sqrt{\beta} x_{WD}\right) = \bar{c}_5 e^{-\sqrt{\beta} x_{WD}} \tag{B17}$$

Now use the discontinuity of the first derivative at the well

$$\left.\frac{\partial \bar{\bar{s}}_D'}{\partial x_D}\right|_{x_D = x_{WD} + dx} - \left.\frac{\partial \bar{\bar{s}}_D'}{\partial x_D}\right|_{x_D = x_{WD} - dx} + 4\pi \bar{Q}_D = 0 \tag{B18}$$

$$-\sqrt{\beta}\bar{c}_5 e^{-\sqrt{\beta} x_{WD}} - \left(\sqrt{\beta}\bar{c}_3 \sinh\left(\sqrt{\beta} x_{WD}\right) + \sqrt{\beta}\bar{c}_4 \cosh\left(\sqrt{\beta} x_{WD}\right)\right) + 4\pi \bar{Q}_D = 0 \tag{B19}$$

$$\bar{c}_5 e^{-\sqrt{\beta} x_{WD}} + \bar{c}_3 \sinh\left(\sqrt{\beta} x_{WD}\right) + \bar{c}_4 \cosh\left(\sqrt{\beta} x_{WD}\right) + \frac{4\pi \bar{Q}_D}{\sqrt{\beta}} = 0 \tag{B20}$$

We have five unknowns and five Eqs. (B14) to (B17) and (B20), so we can solve for c_1, c_2, c_3, c_4, and c_5.

$$\bar{c}_1 = \hat{\bar{H}}_{SD} \tag{B21}$$

$$\bar{c}_2 = -\hat{\bar{H}}_{SD} \frac{\sqrt{\beta}\cosh\left(\sqrt{\mu p} B_D'\right) + \lambda\sqrt{\mu p}\sinh\left(\sqrt{\mu p} B_D'\right)}{\sqrt{\beta}\sinh\left(\sqrt{\mu p} B_D'\right) + \lambda\sqrt{\mu p}\cosh\left(\sqrt{\mu p} B_D'\right)} + \frac{4\pi \bar{Q}_D e^{-\sqrt{\beta} x_{WD}}}{\sqrt{\beta}\sinh\left(\sqrt{\mu p} B_D'\right) + \lambda\sqrt{\mu p}\cosh\left(\sqrt{\mu p} B_D'\right)} \tag{B22}$$

$$\bar{c}_3 = \hat{\bar{H}}_{SD} \frac{\lambda\sqrt{\mu p}}{\sqrt{\beta}\sinh\left(\sqrt{\mu p} B_D'\right) + \lambda\sqrt{\mu p}\cosh\left(\sqrt{\mu p} B_D'\right)} + \frac{4\pi \bar{Q}_D e^{-\sqrt{\beta} x_{WD}} \sinh\left(\sqrt{\mu p} B_D'\right)}{\sqrt{\beta}\sinh\left(\sqrt{\mu p} B_D'\right) + \lambda\sqrt{\mu p}\cosh\left(\sqrt{\mu p} B_D'\right)} \tag{B23}$$

$$\bar{c}_4 = -\hat{\bar{H}}_{SD}\frac{\lambda\sqrt{\mu p}}{\sqrt{\beta}\sinh\left(\sqrt{\mu p}B'_D\right)+\lambda\sqrt{\mu p}\cosh\left(\sqrt{\mu p}B'_D\right)} + \frac{4\pi\bar{Q}_D\lambda\sqrt{\mu p}e^{-\sqrt{\beta}x_{WD}}\cosh\left(\sqrt{\mu p}B'_D\right)}{\sqrt{\beta}\left[\sqrt{\beta}\sinh\left(\sqrt{\mu p}B'_D\right)+\lambda\sqrt{\mu p}\cosh\left(\sqrt{\mu p}B'_D\right)\right]} \tag{B24}$$

$$\bar{c}_5 = \hat{\bar{H}}_{SD}\frac{\lambda\sqrt{\mu p}}{\sqrt{\beta}\sinh\left(\sqrt{\mu p}B'_D\right)+\lambda\sqrt{\mu p}\cosh\left(\sqrt{\mu p}B'_D\right)} + \frac{4\pi\bar{Q}_D\left[\sqrt{\beta}\cosh\left(\sqrt{\beta}x_{WD}\right)\sinh\left(\sqrt{\mu p}B'_D\right)+\lambda\sqrt{\mu\beta}\sinh\left(\sqrt{\beta}x_{WD}\right)\cosh\left(\sqrt{\mu p}B'_D\right)\right]}{\sqrt{\beta}\left[\sqrt{\beta}\sinh\left(\sqrt{\mu p}B'_D\right)+\lambda\sqrt{\mu p}\cosh\left(\sqrt{\mu p}B'_D\right)\right]} \tag{B25}$$

Substituting $\bar{c}_1, \bar{c}_2, \bar{c}_3, \bar{c}_4$ and $\bar{c}_5$ into Eqs. (B10), (B11), and (B12), the results are shown in Eqs. (2.22), (2.23), and (2.24).

APPENDIX C

Appendix C show determination of ω_n and μ_n.

The one-dimensional steady-state flow equation in streambed 2 is

$$\frac{\partial^2 s_{2D}}{\partial^2 x_D^2} = 0. \tag{C1}$$

Considering the boundary condition of $s_{2D}(x_D = 1 + B_{2D}) = 0$, one has

$$s_{2D} = \lambda_2 (1 + B_{2D} - x_D), \tag{C2}$$

where λ_2 is a constant. From the boundary condition Eq. (3.3.) at x_D=1, one has

$$\lambda_2 = \frac{s_D(x_D = 1)}{B_{2D}}. \tag{C3}$$

Substituting Eq. (C2) into Eq. (3.3.) and applying (C3), one obtains

$$-\frac{1}{B_{2D}} \sum_{n=0}^{\infty} \left[\frac{2\pi}{\alpha_n \omega_n} \sin(\omega_n + \mu_n) \sin(\omega_n a_D + \mu_n) \exp(-\omega_n |y_D|) \right]$$
$$= \beta_2 \sum_{n=0}^{\infty} \left[\frac{2\pi}{\alpha_n \omega_n} \omega_n \cos(\omega_n + \mu_n) \sin(\omega_n a_D + \mu_n) \exp(-\omega_n |y_D|) \right]. \tag{C4}$$

Considering the orthogonality of the sine function in (C4), one has

$$-\frac{1}{B_{2D}} \sin(\omega_n + \mu_n) = \beta_2 \omega_n \cos(\omega_n + \mu_n), \tag{C5}$$

or

$$\tan(\omega_n + \mu_n) = -B_{2D} \beta_2 \omega_n. \tag{C6}$$

The one-dimensional steady-state flow equation in the streambed 1 is

$$\frac{\partial^2 s_{1D}}{\partial^2 x_D^2} = 0. \tag{C7}$$

The general solution to this equation by taking into account the boundary condition $s_{1D}(x_D = -B_{1D}) = 0$ is

$$s_{1D} = \lambda_1(B_{1D} + x_D). \tag{C8}$$

From Eq. (3.3.) at x_D=0, one has

$$\lambda_1 = \frac{s_D(x_D = 0)}{B_{1D}}. \tag{C9}$$

Substituting Eq. (C8) into Eq. (3.3.) and applying Eq. (C9), one gets

$$\frac{1}{B_{1D}} \sum_{n=0}^{\infty} \left[\frac{2\pi}{\alpha_n \omega_n} \sin(\mu_n) \sin(\omega_n a_D + \mu_n) \exp(-\omega_n |y_D|) \right]$$

$$= \beta_1 \sum_{n=0}^{\infty} \left[\frac{2\pi}{\alpha_n \omega_n} \omega_n \cos(\mu_n) \sin(\omega_n a_D + \mu_n) \exp(-\omega_n |y_D|) \right]. \tag{C10}$$

Similarly, using the orthogonality of the sine function in (C10) results in

$$\frac{1}{B_{1D}} \sin(\mu_n) = \beta_1 \omega_n \cos(\mu_n), \tag{C11}$$

or

$$\tan(\mu_n) = B_{1D} \beta_1 \omega_n. \tag{C12}$$

Expanding $\tan(\omega_n + \mu_n)$ in Eq. (C6) to terms of $\tan(\omega_n)$ and $\tan(\mu_n)$, and considering Eq. (C12) will result in

$$\tan(\omega_n) = \frac{(B_{1D}\beta_1 + B_{2D}\beta_2)}{(B_{1D}\beta_1 B_{2D}\beta_2 \omega_n^2 - 1)} \omega_n \tag{C13}$$

ω_n is then be computed numerically by solving Eq. (C13). After that, μ_n is obtained from (C12) as $\mu_n = \tan^{-1}(B_{2D}\beta_2\omega_n)$.

VITA

Name:	Trin Intaraprasong
Address:	259/45 Sukimvit 71 road, Prakanong, Bangkok, Thailand, 10110
Education:	B.S., Earth Science, University of California, Santa Cruz, 2001 Ph.D., Geology, Texas A&M University, 2007
Research interest:	Stream aquifer interaction, GIS application in groundwater and surface water, flood, subsidence